iScience

CellPress
OPEN ACCESS

Article

An Amyotrophic Lateral Sclerosis-Associated Mutant of C21ORF2 Is Stabilized by NEK1-Mediated Hyperphosphorylation and the Inability to Bind FBXO3

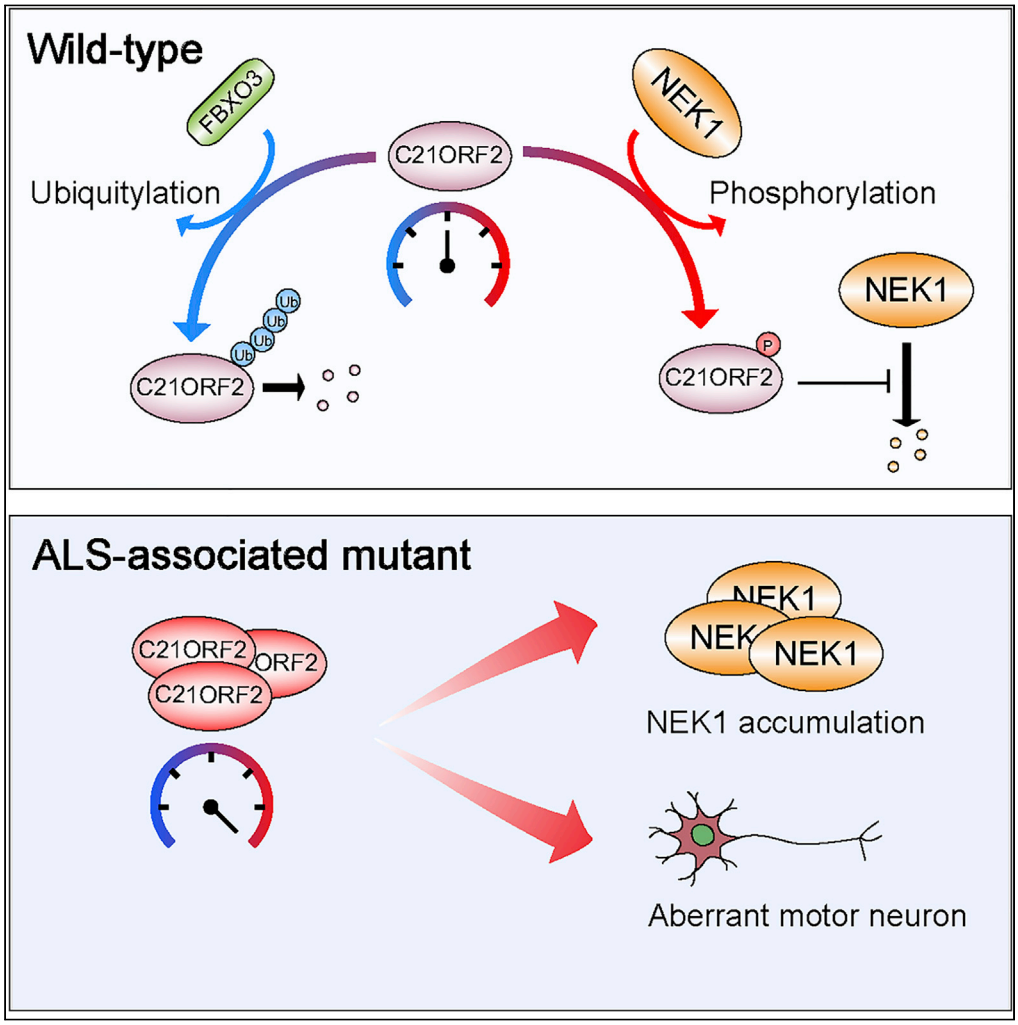

Yasuaki Watanabe, Tadashi Nakagawa, Tetsuya Akiyama, ..., Hitoshi Warita, Masashi Aoki, Keiko Nakayama

nakayak2@med.tohoku.ac.jp

HIGHLIGHTS

C21ORF2 is a common substrate of FBXO3 and NEK1

NEK1-mediated phosphorylation of C21ORF2 inhibits its ubiquitylation and degradation

ALS-associated mutant of C21ORF2 is stable owing to hyperphosphorylation

The C21ORF2 mutant protein causes NEK1 accumulation and motor neuron abnormality

Watanabe et al., iScience *23*, 101491
September 25, 2020
https://doi.org/10.1016/j.isci.2020.101491

iScience

CellPress
OPEN ACCESS

Article

An Amyotrophic Lateral Sclerosis-Associated Mutant of C21ORF2 Is Stabilized by NEK1-Mediated Hyperphosphorylation and the Inability to Bind FBXO3

Yasuaki Watanabe,[1,2] Tadashi Nakagawa,[2] Tetsuya Akiyama,[1] Makiko Nakagawa,[2] Naoki Suzuki,[1] Hitoshi Warita,[1] Masashi Aoki,[1] and Keiko Nakayama[2,3,*]

SUMMARY

***C21ORF2* and *NEK1* have been identified as amyotrophic lateral sclerosis (ALS)-associated genes. Both genes are also mutated in certain ciliopathies, suggesting that they might contribute to the same signaling pathways. Here we show that FBXO3, the substrate receptor of an SCF ubiquitin ligase complex, binds and ubiquitylates C21ORF2, thereby targeting it for proteasomal degradation. C21ORF2 stabilizes the kinase NEK1, with the result that loss of FBXO3 stabilizes not only C21ORF2 but also NEK1. Conversely, NEK1-mediated phosphorylation stabilizes C21ORF2 by attenuating its interaction with FBXO3. We found that the ALS-associated V58L mutant of C21ORF2 is more susceptible to phosphorylation by NEK1, with the result that it is not ubiquitylated by FBXO3 and therefore accumulates together with NEK1. Expression of C21ORF2(V58L) in motor neurons induced from mouse embryonic stem cells impaired neurite outgrowth. We suggest that inhibition of NEK1 activity is a potential therapeutic approach to ALS associated with *C21ORF2* mutation.**

INTRODUCTION

Dysfunction of systems responsible for protein quality control as well as altered RNA metabolism has been implicated in the pathogenesis of amyotrophic lateral sclerosis (ALS) (Ling et al., 2013; Shahheydari et al., 2017). The ubiquitin-proteasome system is essential for maintenance of protein homeostasis at the level of protein degradation. Indeed, various neurodegenerative diseases including ALS are characterized pathologically by the formation of inclusion bodies consisting of insoluble and unfolded proteins tagged with ubiquitin, suggesting that a defect in or overload of the ubiquitin-proteasome system may play an important role in the formation of these structures (Ardley and Robinson, 2004; Neumann et al., 2006).

The E3 ubiquitin ligases mediate the transfer of ubiquitin to substrate proteins and include CRL1 ligases, also known as S phase kinase associated protein 1 (SKP1)–Cullin 1 (CUL1)-F box protein (SCF) complexes (Wang et al., 2014). In each SCF complex, the COOH terminus of the scaffold protein CUL1 binds the RING-finger protein RBX1 and thereby recruits an E2 enzyme, whereas the NH_2 terminus of CUL1 binds SKP1 and an associated F box protein, the latter of which is responsible for substrate recognition (Skaar et al., 2013). The F box domain of F box proteins mediates direct binding to SKP1 (Bai et al., 1996). Approximately 70 F box proteins have been identified in humans, each of which specifically recognizes a distinct group of substrates, with the result that SCF complexes mediate the ubiquitylation and degradation of a large variety of proteins (Nakagawa et al., 2020; Nakayama and Nakayama, 2006). F box proteins are categorized into three classes on the basis of their substrate interaction domains: FBXW proteins (which contain WD40 repeat domains), FBXL proteins (which contain leucine-rich repeat [LRR] domains), and FBXO proteins (whose protein interaction domains are poorly characterized) (Jin et al., 2004).

ALS is characterized by the selective dysfunction and loss of motor neurons (Brown and Al-Chalabi, 2017). Most knowledge of ALS pathogenesis has been obtained by functional analysis of causal or risk genes (Chia et al., 2018; Weishaupt et al., 2016). A recent genome-wide association study and meta-analysis identified the chromosome 21 open reading frame 2 gene (*C21ORF2*) as being associated with ALS (van Rheenen et al., 2016). The C21ORF2 protein contains thee highly conserved LRR domains (Scott et al., 1998), but the function of these repeats and that of C21ORF2 itself remain largely unexplored. C21ORF2 is known

[1]Department of Neurology, Graduate School of Medicine, Tohoku University, Sendai, Miyagi 980-8575, Japan

[2]Division of Cell Proliferation, ART, Graduate School of Medicine, Tohoku University, Sendai, Miyagi 980-8575, Japan

[3]Lead Contact

*Correspondence: nakayak2@med.tohoku.ac.jp

https://doi.org/10.1016/j.isci.2020.101491

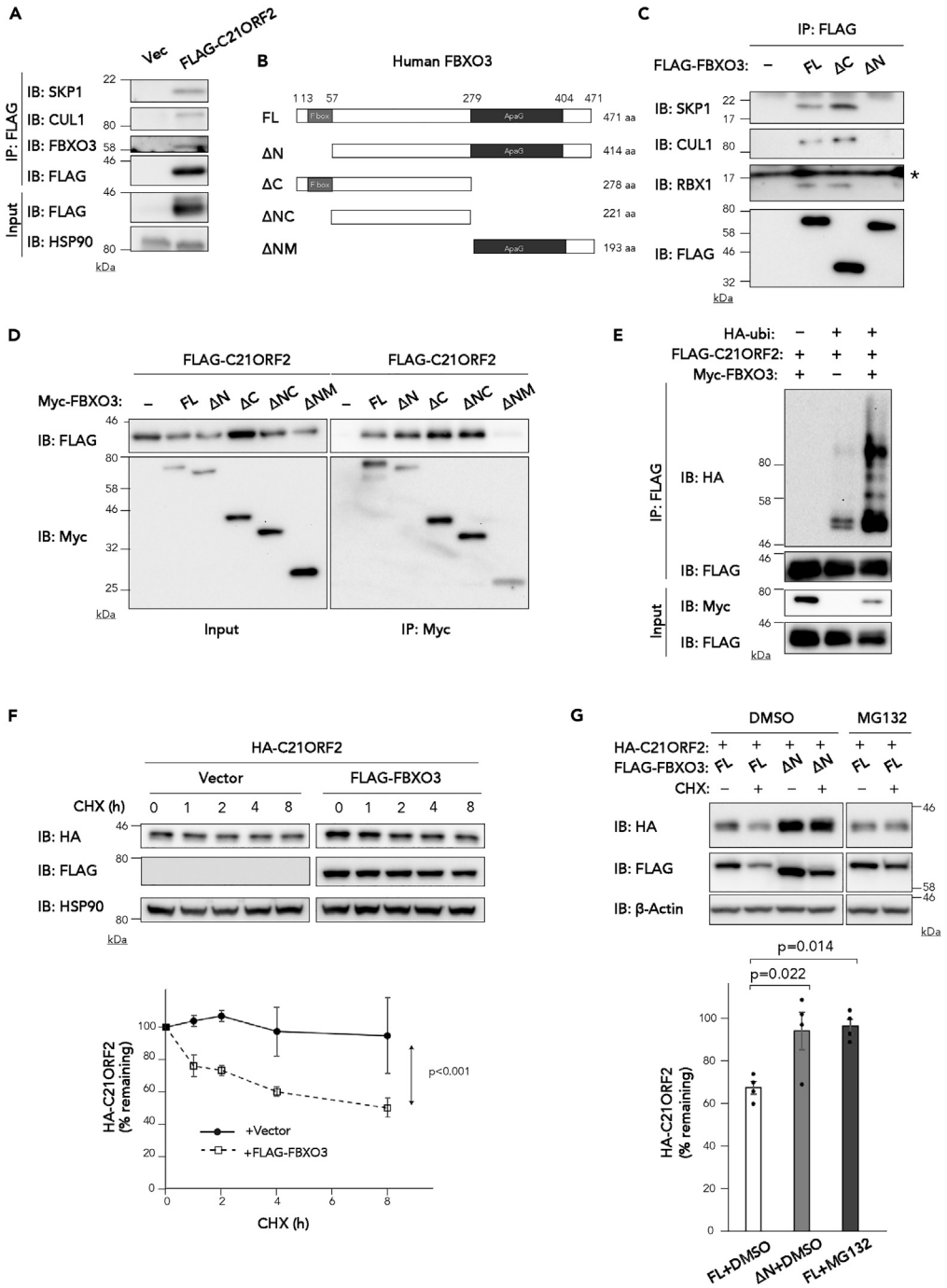

Figure 1. C21ORF2 Is a Substrate of SCF^{FBXO3}

(A) Lysates of HEK293T cells expressing FLAG-C21ORF2 or transfected with the corresponding empty vector (Vec) were subjected to immunoprecipitation (IP) with antibodies to FLAG, and the resulting precipitates as well as the original cell lysates (Input) were subjected to immunoblot (IB) analysis with antibodies to SKP1, CUL1, FBXO3, FLAG, and HSP90 (loading control).

(B) Schematic representation of truncated variants of human FBXO3. The F box and ApaG domains are indicated. aa, amino acids.

(C) Lysates of HEK293T cells expressing FLAG-tagged FBXO3 variants (FL, ΔC, or ΔN) were subjected to immunoprecipitation with antibodies to FLAG, and the resulting precipitates were subjected to immunoblot analysis with antibodies to SCF components (SKP1, CUL1, and RBX1) and FLAG. The asterisk indicates nonspecific bands.

Figure 1. *Continued*

(D) Lysates of HEK293T cells expressing FLAG-C21ORF2 and Myc epitope-tagged FBXO3 variants (FL, ΔN, ΔC, ΔNC, or ΔNM) were subjected to immunoprecipitation with antibodies to Myc, and the resulting precipitates as well as the original cell lysates were subjected to immunoblot analysis with antibodies to FLAG and Myc.

(E) Lysates of HEK293T cells expressing HA-tagged ubiquitin (ubi), FLAG-C21ORF2, and Myc-FBXO3, as indicated, were subjected to immunoprecipitation with antibodies to FLAG, and the resulting precipitates as well as the original cell lysates were subjected to immunoblot analysis with antibodies to HA, FLAG, and Myc.

(F) HEK293T cells expressing HA-C21ORF2 with or without FLAG-FBXO3 were treated with cycloheximide (CHX, 25 μg/mL) for the indicated times, lysed, and subjected to immunoblot analysis with antibodies to HA, FLAG, and HSP90. Representative immunoblots (upper) as well as quantitative analysis of the band intensity for HA-C21ORF2 normalized by that for HSP90 (lower) are shown. Quantitative data are mean ± SEM values from three independent experiments. The p value was determined by two-way ANOVA.

(G) HEK293T cells coexpressing HA-C21ORF2 and FLAG-FBXO3 (FL or ΔN) were incubated in the absence or presence of cycloheximide (25 μg/mL) or 10 μM MG132 (or dimethyl sulfoxide [DMSO] vehicle) for 4 h, lysed, and subjected to immunoblot analysis with antibodies to HA, FLAG, and β-actin (loading control). Representative immunoblots (upper) as well as quantitative analysis of the percentage of HA-C21ORF2 remaining (normalized by β-actin) in cycloheximide-treated cells compared with the corresponding cells without cycloheximide treatment (lower) are shown. Quantitative data are mean ± SEM values from four independent experiments. The p value was determined by one-way ANOVA followed by Tukey's post hoc test.

See also Figure S1.

to form a functional complex with NEK1 (never in mitosis gene A related kinase 1) (Wheway et al., 2015). Several homozygous mutations of *C21ORF2* and of *NEK1* have been identified in individuals with ciliopathies, a group of genetic disorders caused by a defect of primary cilia (Thiel et al., 2011; Wheway et al., 2015). Case-control studies have also revealed that certain missense or loss-of-function mutations of *NEK1* are more frequent in individuals with familial or sporadic ALS in European countries and China (Brenner et al., 2016; Gratten et al., 2017; Kenna et al., 2016). NEK1 possesses both serine-threonine and tyrosine kinase activities *in vitro* (Letwin et al., 1992), and it functions in the repair of DNA damage and in cell cycle regulation (Chen et al., 2008; Fry et al., 2012; Melo-Hanchuk et al., 2017). C21ORF2 and NEK1 may therefore play a cooperative and key role in ALS pathogenesis by contributing to the same signaling pathways.

We have now identified C21ORF2 as a substrate of F box only protein 3 (FBXO3). The SKP1-CUL1-FBXO3 (SCF^{FBXO3}) complex ubiquitylates and thereby triggers the degradation of C21ORF2, but the binding of FBXO3 to C21ORF2 is prevented by NEK1-mediated phosphorylation of C21ORF2. Phosphorylation by NEK1 thus stabilizes the C21ORF2 protein. In a reciprocal manner, we also found that C21ORF2 stabilizes NEK1. Of note, the protein encoded by an ALS-associated mutant form of *C21ORF2*, C21ORF2(V58L), is not a substrate of SCF^{FBXO3}. Furthermore, mouse embryonic stem cell (ESC)-derived induced motor neurons (iMNs) harboring the corresponding heterozygous missense mutation of mouse *C21orf2* manifested a reduced neurite length. Our findings provide biological evidence that C21ORF2 degradation mediated by SCF^{FBXO3} determines the abundance of NEK1 and contributes to the phenotype of motor neurons.

RESULTS

C21ORF2 Is a Substrate of SCF^{FBXO3}

To investigate the molecular function of C21ORF2 (also known as CFAP410) and its role in ALS pathogenesis, we searched for proteins that associate with C21ORF2. Analysis of published data for C21ORF2-binding proteins identified by affinity purification combined with mass spectrometry revealed that such proteins included SKP1, CUL1, and FBXO3 (Wheway et al., 2015). To validate this finding, we subjected immunoprecipitates of FLAG epitope-tagged C21ORF2 expressed in HEK293T cells to immunoblot analysis. We detected SKP1, CUL1, and FBXO3 in the immunoprecipitates, thereby confirming the interaction between these proteins and C21ORF2 (Figure 1A). Immunoprecipitation analysis with a series of truncated mutants of FBXO3 also confirmed that the F box domain is responsible for binding to the SKP1-CUL1-RBX1 catalytic module of SCF^{FBXO3} (Figures 1B and 1C), consistent with the general features of F box proteins (Bai et al., 1996). In addition, immunoprecipitation analysis revealed that an FBXO3 mutant comprising amino acids 58 to 278 (ΔNC) bound C21ORF2, whereas FBXO3(ΔNM), consisting of the COOH-terminal 193 amino acids, did not, indicating that residues 58–278 of FBXO3 are responsible for binding to C21ORF2 (Figures 1B and 1D). To test whether C21ORF2 is ubiquitylated by SCF^{FBXO3}, we first examined the ubiquitylation level of C21ORF2 in cells with or without FBXO3 overexpression. Such *in vivo* ubiquitylation analysis showed that FBXO3 overexpression increased the ubiquitylation level of C21ORF2 (Figure 1E). Moreover,

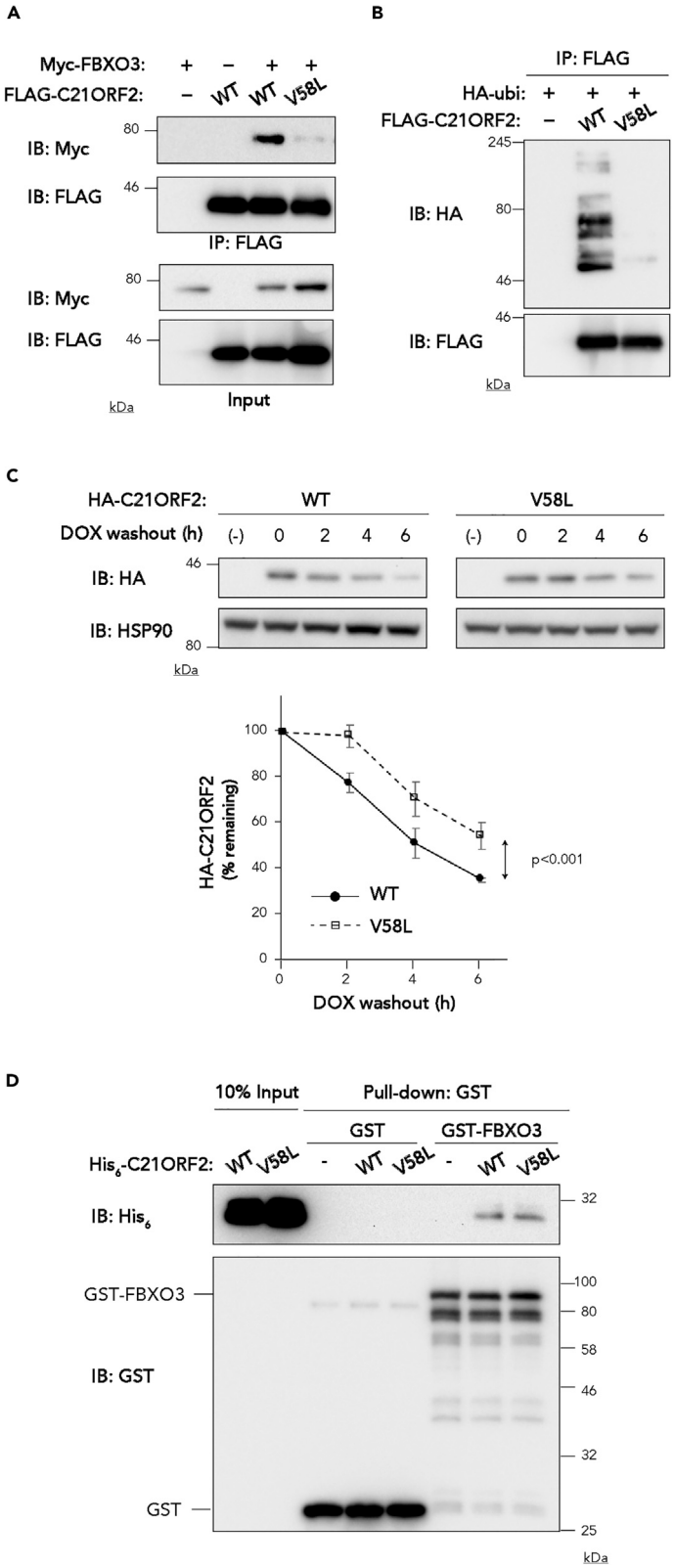
A
Myc-FBXO3: + − + +
FLAG-C21ORF2: − WT WT V58L
IB: Myc
IB: FLAG
IP: FLAG
IB: Myc
IB: FLAG
Input
kDa
B
IP: FLAG
HA-ubi: + + +
FLAG-C21ORF2: − WT V58L
IB: HA
IB: FLAG
kDa
C
HA-C21ORF2: WT V58L
DOX washout (h) (-) 0 2 4 6 (-) 0 2 4 6
IB: HA
IB: HSP90
kDa
HA-C21ORF2 (% remaining)
p<0.001
WT
V58L
DOX washout (h)
D
10% Input
Pull-down: GST
GST
GST-FBXO3
His6-C21ORF2: WT V58L - WT V58L - WT V58L
IB: His6
GST-FBXO3
IB: GST
GST
kDa

Figure 2. The ALS-Associated V58L Mutant of C21ORF2 Is not a Substrate of SCF^{FBXO3}

(A) Immunoprecipitation and immunoblot analysis of the interaction between FLAG-tagged C21ORF2 (WT or V58L) and Myc-tagged FBXO3 in HEK293T cells.

(B) *In vivo* ubiquitylation analysis of FLAG-tagged C21ORF2 (WT or V58L) in HEK293T cells.

(C) SH-SY5Y cells engineered to express HA-tagged C21ORF2 (WT or V58L) on exposure to DOX were incubated with or without (−) DOX (1 μg/mL) for 2 days. The cells cultured with DOX were then incubated without DOX for the indicated times, after which they were lysed and subjected to immunoblot analysis with antibodies to HA and HSP90. Representative blots (upper) and quantitative analysis of the band intensity for HA-C21ORF2 normalized by that for HSP90 (lower) are shown. Quantitative data are means ± SEM from three independent experiments. The p value was determined by two-way ANOVA.

(D) *In vitro* binding assay for glutathione S-transferase (GST)-tagged FBXO3 and His_6-tagged C21ORF2 (WT or V58L). The recombinant proteins were incubated together overnight at 4°C, after which GST or GST-FBXO3 removed by precipitation with glutathione beads as well as a portion of the His_6-C21ORF2 input (10%) were subjected to immunoblot analysis with antibodies to His_6 and to GST.

See also Figure S2.

treatment of cells with the proteasome inhibitor MG132 induced the accumulation of C21ORF2 and increased its ubiquitylation level, suggesting that ubiquitylated C21ORF2 is degraded by the proteasome (Figure S1A). We then determined the rate of C21ORF2 degradation in HEK293T cells by blocking protein synthesis with cycloheximide. We found that hemagglutinin epitope (HA)-tagged C21ORF2 was degraded more rapidly in cells overexpressing FBXO3 than in control cells, suggesting that FBXO3 promotes C21ORF2 degradation (Figure 1F). Furthermore, in contrast to cells expressing full-length (FL) FBXO3, cycloheximide treatment did not reveal degradation of C21ORF2 in cells expressing FBXO3(ΔN), which is unable to interact with SKP1 (Figure 1G). We confirmed that proteasome inhibition by MG132 attenuated the degradation of C21ORF2 apparent in cells overexpressing FBXO3(FL) after their exposure to cycloheximide (Figure 1G). Together, these observations indicated that FBXO3 promotes C21ORF2 degradation in a manner dependent on the catalytic activity of both SCF^{FBXO3} and the proteasome.

To identify the sites of C21ORF2 ubiquitylation, we expressed a mutant protein in which all eight lysine residues were replaced with arginine (8KR) in HEK293T cells (Figure S1B). However, we found that the 8KR mutant was ubiquitylated at a level similar to that apparent for the wild-type (WT) protein (Figure S1C), suggesting that C21ORF2 is ubiquitylated at sites other than lysine residues, possibly including the NH_2-terminal amine group (McDowell and Philpott, 2013).

The ALS-Associated V58L Mutant of C21ORF2 Is Not a Substrate of SCF^{FBXO3}

An ALS-associated missense mutation of C21ORF2 results in a V58L substitution in the second of the three LRRs (van Rheenen et al., 2016) (Figure S2A). We tested whether this mutant protein is also a substrate of SCF^{FBXO3}. FBXO3 bound to the NH_2-terminal region of C21ORF2(WT) containing the LRRs as well as to the corresponding COOH-terminal region containing the LRR COOH-terminal (LRRCT) domain (Figure S2), whereas FBXO3 did not bind to C21ORF2(V58L) and the mutant protein was not ubiquitylated in HEK293T cells (Figures 2A and 2B), suggesting that FBXO3 is the only ubiquitin ligase for C21ORF2 and that the ALS-related V58L mutation prevents the ubiquitylation of C21ORF2. Given that SCF^{FBXO3} targets C21ORF2 for proteasomal degradation, C21ORF2(V58L) might be expected to be more stable than the WT protein. To compare the stability of the WT and V58L proteins in neuronal cells, we generated SH-SY5Y cell lines in which the expression of HA-tagged forms of these proteins was inducible by doxycycline (DOX) with the use of the Tet-on system (rtTA-TetP-HA-C21ORF2-WT and -V58L, respectively). The cells were incubated with DOX for 2 days to induce the expression of C21ORF2(WT) or C21ORF2(V58L), after which further transcription was blocked by removal of DOX and the cells were subjected to immunoblot analysis 2, 4, or 6 h later. The percentage amount of C21ORF2(V58L) remaining during the time course was significantly greater than that of C21ORF2(WT) (Figure 2C), indicating that C21ORF2(V58L) is indeed more stable than is C21ORF2(WT) as a result of not being a substrate of SCF^{FBXO3}.

To confirm that C21ORF2 binds FBXO3 directly and that the V58L mutation of C21ORF2 disrupts this binding, we performed a pull-down assay with recombinant proteins expressed in and purified from *Escherichia coli*. Unexpectedly, we found that not only C21ORF2(WT) but also the V58L mutant bound to FBXO3 (Figure 2D). Given that SCF complexes often recognize substrates in a modification-dependent manner (Skaar et al., 2013), this finding suggested the possibility that either posttranslational modification such as phosphorylation of C21ORF2 or some other molecule regulates the interaction between C21ORF2 and FBXO3.

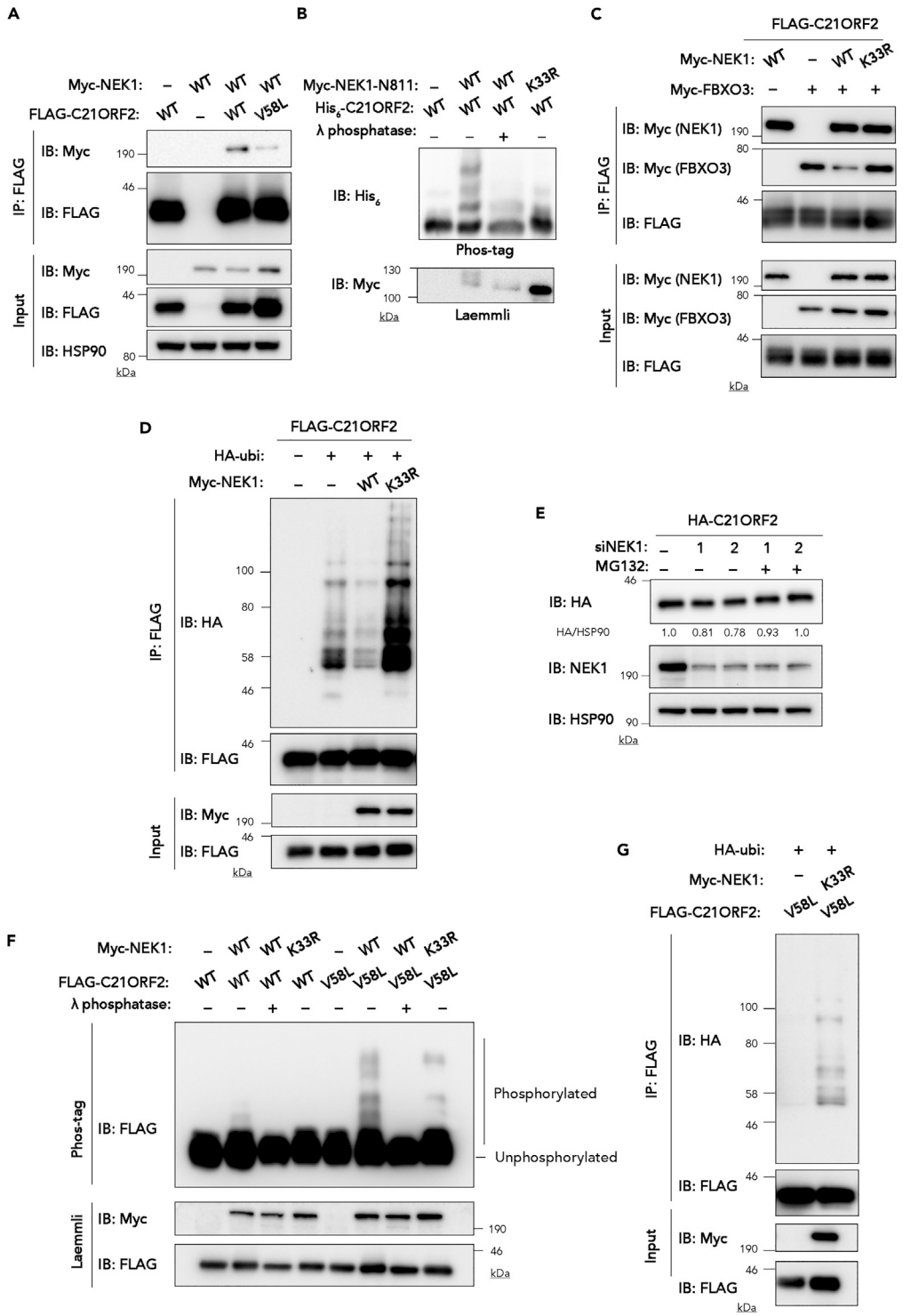

Figure 3. FBXO3-Mediated C21ORF2 Ubiquitylation Is Negatively Regulated by NEK1

(A) Immunoprecipitation and immunoblot analysis of the interaction between FLAG-tagged C21ORF2 (WT or V58L) and Myc-tagged NEK1 in HEK293T cells.

(B) *In vitro* kinase assay of recombinant His_6-C21ORF2 phosphorylation by Myc-tagged NEK1-N811 (WT or K33R) immunoprecipitates prepared from HEK293T cells. The reaction was performed for 15 min at 30°C, after which the

Figure 3. *Continued*
reaction mixtures were treated (or not) with λ phosphatase and then subjected to Phos-tag or Laemmli SDS-PAGE followed by immunoblot analysis with antibodies to His_6 and Myc.
(C) Immunoprecipitation and immunoblot analysis of the effect of Myc-tagged NEK1 (WT or K33R) expression on the interaction of FLAG-C21ORF2 with Myc-FBXO3 in HEK293T cells. Myc-FBXO3 and Myc-NEK1 were distinguished on the basis of molecular size.
(D) *In vivo* assay of the effect of Myc-tagged NEK1 (WT or K33R) expression on the ubiquitylation of FLAG-C21ORF2 in HEK293T cells.
(E) HEK293T cells were transfected first with two different small interfering RNAs (siRNAs) for NEK1 or with a control siRNA (day 1) and then with an expression vector for HA-C21ORF2 (day 2), incubated with 10 μM MG132 or DMSO vehicle for 3 h (day 3), lysed, and subjected to immunoblot analysis with antibodies to HA and NEK1. The band intensity for HA-C21ORF2 (normalized by that of HSP90) was quantified by densitometry.
(F) HEK293T cells expressing FLAG-tagged C21ORF2 (WT or V58L) and Myc-tagged NEK1 (WT or K33R) were lysed, treated (or not) with λ phosphatase, and subjected to Phos-tag or Laemmli SDS-PAGE followed by immunoblot analysis with antibodies to FLAG and Myc.
(G) *In vivo* assay of the effect of Myc-NEK1(K33R) expression on the ubiquitylation of FLAG-C21ORF2(V58L) in HEK293T cells.

The Interaction between FBXO3 and C21ORF2 Is Prevented by NEK1-Mediated Phosphorylation of C21ORF2

Given that NEK1 was previously shown to bind C21ORF2 and is implicated in the pathogenesis of ALS, we examined whether NEK1 might phosphorylate C21ORF2 and thereby regulate its interaction with FBXO3. Immunoprecipitation analysis showed that both C21ORF2(WT) and C21ORF2(V58L) bound NEK1 in HEK293T cells, although the extent of the interaction with NEK1 was less pronounced for the V58L mutant than for C21ORF2(WT) (Figure 3A). To investigate whether NEK1 directly phosphorylates C21ORF2, we performed an *in vitro* kinase assay with recombinant C21ORF2 purified from bacteria and an immunoprecipitated fragment of NEK1 that consists of the NH_2-terminal 811 amino acids and includes the kinase domain. Phos-tag SDS-poylacrylamide gel electrophoresis (PAGE), which separates phosphorylated forms of proteins as higher molecular mass bands (Kinoshita et al., 2009), revealed multiple upward band shifts of C21ORF2(WT) after its incubation with NEK1-N811 and ATP (Figure 3B). Such band shifts were not detected after treatment of the reaction mixture with lambda (λ) phosphatase or in the presence of the kinase-dead K33R mutant of NEK1-N811 instead of the WT fragment, suggesting that C21ORF2(WT) was phosphorylated at multiple sites by NEK1. Of note, overexpression of NEK1(WT) inhibited the binding of C21ORF2 to FBXO3 as well as attenuated the ubiquitylation of C21ORF2 in HEK293T cells, whereas forced expression of NEK1(K33R) increased both C21ORF2-FBXO3 binding and C21ORF2 ubiquitylation (Figures 3C and 3D). These results suggested that the FBXO3-mediated ubiquitylation of C21ORF2 is negatively regulated by NEK1-dependent phosphorylation of C21ORF2. In addition, NEK1 knockdown resulted in a reduction in the abundance of C21ORF2 in HEK293T cells, and this effect was prevented by proteasome inhibition induced by MG132 treatment (Figure 3E), suggesting that phosphorylation by NEK1 stabilizes C21ORF2 by protecting it from proteasome-dependent degradation.

Given that C21ORF2(V58L) did not bind FBXO3 *in vivo* but did so *in vitro* (Figures 2A and 2D) and that the interaction of NEK1 with C21ORF2(V58L) was less pronounced than was that with C21ORF2(WT) (Figure 3A), we predicted that C21ORF2(V58L) might be phosphorylated to a greater extent by NEK1 compared with C21ORF2(WT), resulting in its inability to bind to and to undergo ubiquitylation by FBXO3 *in vivo*. To assess this possibility, we compared the intracellular phosphorylation levels of C21ORF2(WT) and its V58L mutant. The extent of C21ORF2(V58L) phosphorylation was indeed greater than that of C21ORF2(WT) in HEK293T cells overexpressing NEK1 (Figure 3F). Of note, dominant negative inhibition of endogenous NEK1 function by forced expression of NEK1(K33R) promoted the ubiquitylation of C21ORF2(V58L) (Figure 3G). Together, these data suggested that ubiquitylation of C21ORF2 by SCF^{FBXO3} is negatively regulated by NEK1-mediated phosphorylation of C21ORF2. Moreover, the binding of C21ORF2(V58L) to and its ubiquitylation by FBXO3 *in vivo* are prevented as a result of its increased susceptibility to phosphorylation by NEK1 compared with C21ORF2(WT).

C21ORF2 Stabilizes NEK1

To investigate the cellular function of C21ORF2, we inactivated *C21ORF2* in HEK293T cells with the CRISPR/Cas9 system. We confirmed that C21ORF2 protein was depleted (Figures 4A and S3) and that the amount of *C21ORF2* mRNA was reduced (Figure 4B), probably as a result of nonsense-mediated decay, in two knockout (KO) clones. We noticed that the abundance of endogenous NEK1 protein, but not that of

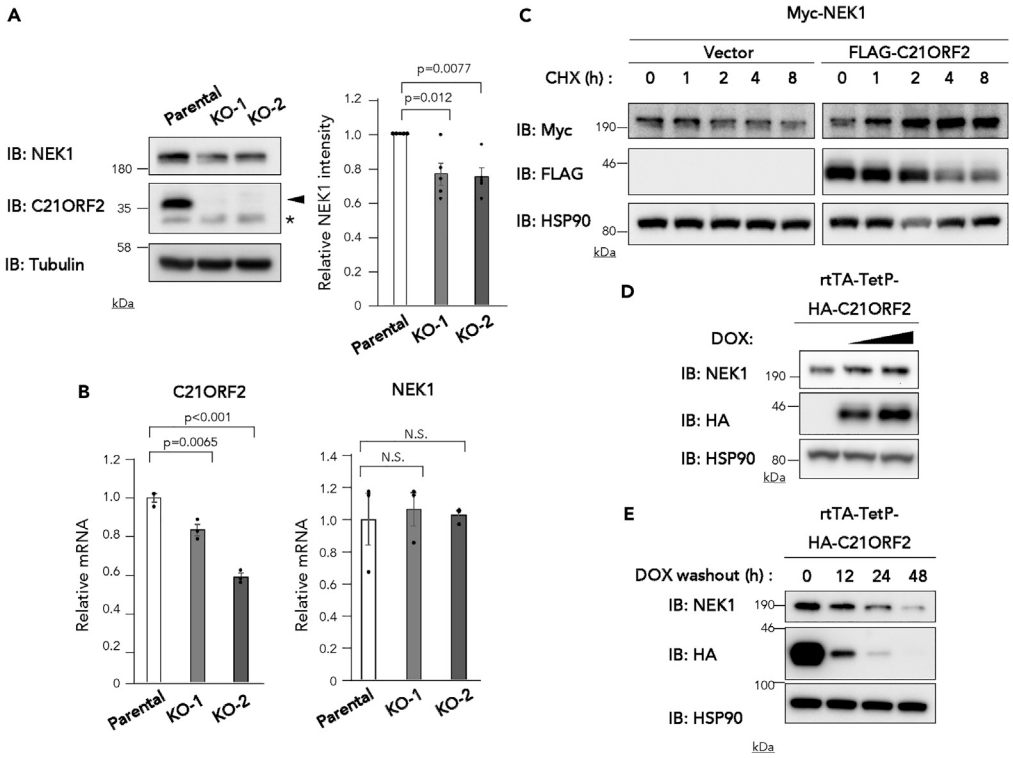

Figure 4. C21ORF2 Stabilizes NEK1

(A) Immunoblot analysis of NEK1 in two *C21ORF2* KO clones of HEK293T cells as well as in the parental cells. Representative immunoblots (left, with the arrowhead indicating the endogenous C21ORF2 band and the asterisk indicating a nonspecific band) and quantification of the band intensity for NEK1 normalized by that of α-tubulin (right) are shown. Quantitative data are means ± SEM for five independent experiments. The p values were determined by one-way ANOVA followed by Tukey's post hoc test.

(B) Reverse transcription (RT) and quantitative polymerase chain reaction (qPCR) analysis of the abundance of *C21ORF2* and *NEK1* mRNAs (normalized by that of *GAPDH* mRNA) in cells as in (A). Data are means ± SEM for three independent experiments. The p values were determined by one-way ANOVA followed by Tukey's post hoc test. N.S., not significant.

(C) Cycloheximide chase analysis of Myc-NEK1 in HEK293T cells expressing (or not) FLAG- C21ORF2.

(D) SH-SY5Y cells engineered to express HA-C21ORF2 on exposure to DOX were incubated with DOX (0, 0.5, or 1 μg/mL) for 2 days, lysed, and subjected to immunoblot analysis with antibodies to NEK1 and HA.

(E) Cells incubated with DOX (1 μg/mL) as in (D) were subsequently incubated in the absence of DOX for 0, 12, 24, or 48 h before immunoblot analysis.

See also Figure S3.

NEK1 mRNA, was also significantly reduced in these *C21ORF2* KO clones (Figures 4A and 4B), suggesting that C21ORF2 stabilizes NEK1 at the protein level. Examination of the dynamics of Myc-NEK1 degradation in cycloheximide-treated HEK293T cells with or without C21ORF2 overexpression revealed that C21ORF2 suppressed the degradation of NEK1 (Figure 4C). Given that C21ORF2(V58L) was more stable than C21ORF2(WT) in SH-SY5Y cells (Figure 2C), we hypothesized that the increased abundance of C21ORF2 that results from such ALS-associated *C21ORF2* mutation might result in an increase in the amount of endogenous NEK1. To test further whether the abundance of endogenous NEK1 is affected by the amount of C21ORF2, we induced the expression of HA-C21ORF2 in engineered SH-SY5Y cells by DOX treatment. We found that the abundance of endogenous NEK1 was indeed increased by such DOX treatment (Figure 4D). Conversely, the abundance of endogenous NEK1 decreased in parallel with the decline in the expression of HA-C21ORF2 in these cells after DOX washout (Figure 4E). Collectively, these results indicated that C21ORF2 stabilizes NEK1 by suppressing its degradation.

C21ORF2 and NEK1 Are Up-Regulated in FBXO3 KO Cells

To examine whether FBXO3 regulates NEK1 abundance indirectly by promoting the proteasomal degradation of C21ORF2, we inactivated *FBXO3* in SH-SY5Y cells with the use of the CRISPR-Cas9 system. We

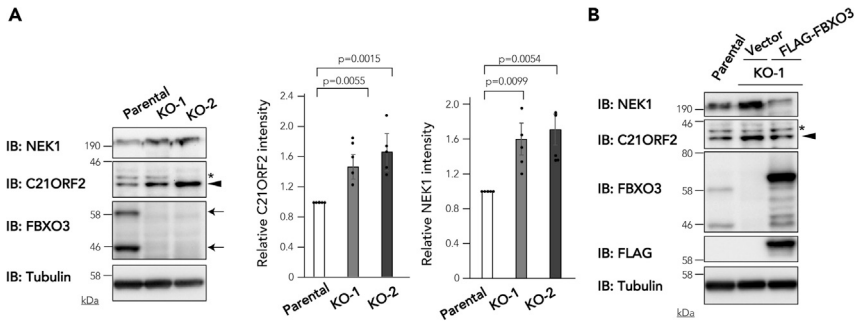

Figure 5. C21ORF2 and NEK1 Are Up-Regulated in *FBXO3* KO Cells

(A) Immunoblot analysis of C21ORF2, NEK1, and FBXO3 in two *FBXO3* KO clones of SH-SY5Y cells as well as in the parental cells. Representative blots (left) and quantitative analysis of the band intensity for C21ORF2 and NEK1 normalized by that for tubulin (right) are shown. The arrowhead and asterisk indicate the band for endogenous C21ORF2 and a nonspecific band, respectively. The arrows indicate the bands for isoforms of endogenous FBXO3. Quantitative data are means ± SEM from five independent experiments. The p values were determined by one-way ANOVA followed by Tukey's post hoc test.

(B) An *FBXO3* KO clone of SH-SY5Y cells was infected with a lentivirus encoding FLAG-FBXO3 or with the corresponding empty virus (Vector), lysed, and subjected to immunoblot analysis with antibodies to NEK1, C21ORF2, FLAG, and FBXO3. The arrowhead and asterisk indicate the band for endogenous C21ORF2 and a nonspecific band, respectively.

See also Figures S4 and S5.

found that the abundance of C21ORF2 protein was increased in two *FBXO3* KO cell clones (Figures 5A and S4), whereas that of *C21ORF2* mRNA was not significantly altered (Figure S5A), consistent with the notion that the loss of FBXO3 results in the stabilization of C21ORF2 protein. The abundance of NEK1 protein was also increased in the *FBXO3* KO cell clones (Figures 5A and S4). Given that the amount of *NEK1* mRNA was also increased in these cells (Figure S5A), both this effect and the accumulation of C21ORF2 protein likely contributed to the up-regulation of NEK1 protein induced by *FBXO3* ablation. The expression of FLAG-FBXO3 in the FBXO3 KO cells reduced the abundance of both C21ORF2 and NEK1 (Figure 5B) without affecting the amounts of the corresponding mRNAs (Figure S5B). Together, these results provide a link between our observations that FBXO3 promotes the proteasomal degradation of C21ORF2 and that C21ORF2 stabilizes NEK1. In other words, our findings suggest that FBXO3 negatively regulates the abundance of both C21ORF2 and NEK1.

Mutation of *C21orf2* Induces NEK1 Stabilization in ESCs and an Aberrant Phenotype in iMNs

Given that the ALS-associated C21ORF2(V58L) mutant is stabilized as a result of its not being targeted by SCF^{FBXO3} for degradation, we hypothesized that the accumulation of the mutant protein might have adverse effects on motor neurons in patients with ALS. To assess this hypothesis, we analyzed the phenotype of motor neurons (iMNs) differentiated from mouse ESCs expressing green fluorescent protein (GFP) under the control of the *Hb9* promoter (Hb9::GFP), which is selectively active in motor neurons (Wichterle et al., 2002). The valine-58 residue of human C21ORF2 that is replaced with leucine in association with ALS is conserved in the mouse protein (Figure 6A). To achieve robust and homogeneous induction of motor neuron differentiation in ESCs, we generated DOX-NIL ESCs, in which polycistronic expression of the transcription factors NGN2, ISL1, and LHX3 (NIL factors) is induced in response to DOX treatment, with these factors having been shown to be sufficient for such differentiation (Mazzoni et al., 2013; Velasco et al., 2017). We then subjected these DOX-NIL ESCs to heterozygous knockin of the V58L mutation of *C21orf2*, thereby generating VLKI ESCs (Figure 6B). The extent of alkaline phosphatase staining (Figure S6A) as well as the amounts of *Oct4* and *Fgf4* mRNAs (Figure S6B) did not differ between VLKI ESCs and the parental DOX-NIL ESCs, indicating that knockin of the *C21orf2* mutation had no effect on ESC pluripotency. Consistent with our finding with HEK293T cells that C21ORF2(V58L) is stabilized as a result of its impaired interaction with FBXO3 (Figure 2), we found that the abundance of endogenous C21ORF2 was increased in VLKI ESCs compared with parental cells (Figure 6C), whereas the amount of *C21orf2* mRNA was reduced in VLKI ESCs (Figure 6D), possibly as a result of negative feedback by the encoded protein. Cycloheximide chase analysis confirmed that total C21ORF2 protein was relatively stable in VLKI ESCs (Figure S6C). We also found that the amount of NEK1 protein was increased in VLKI ESCs (Figure 6C), without an increase in

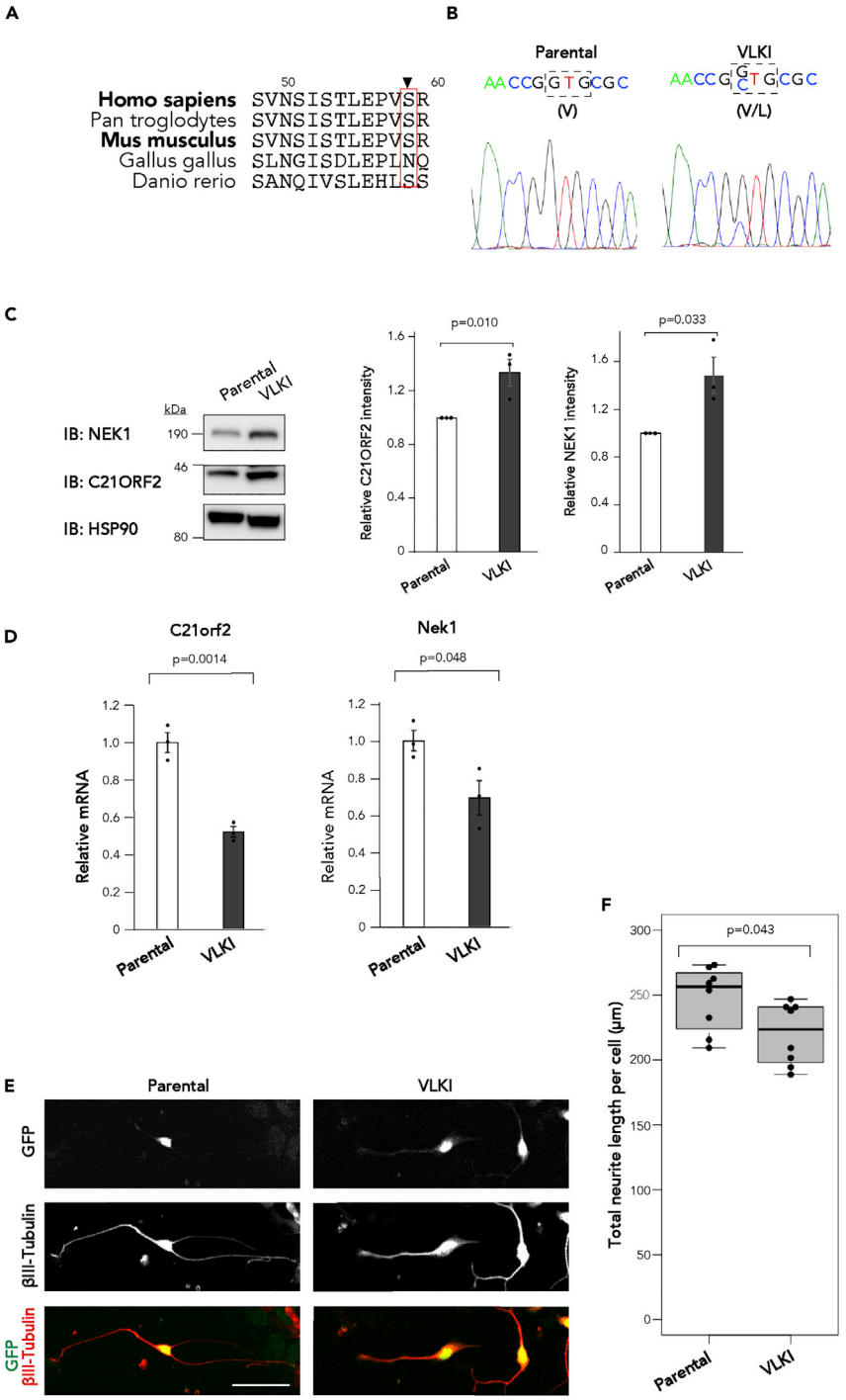

Figure 6. *C21orf2* Mutation Induces NEK1 Stabilization in ESCs and Impairs Neurite Outgrowth in iMNs

(A) Amino acid sequence alignment of vertebrate C21ORF2 orthologs. Residue 58 (arrowhead) is enclosed in the red box.

(B) Sanger sequencing of DNA extracted from parental (DOX-NIL) and VLKI ESCs. The codon for valine-58 of *C21orf2* is shown within the dashed box.

(C) Immunoblot analysis of endogenous C21ORF2 and NEK1 in parental and VLKI ESCs. Representative blots (left) and quantitative analysis of the band intensity for C21ORF2 and NEK1 normalized by that for HSP90 (right) are shown. Quantitative data are means ± SEM from three independent experiments. The p values were determined with Student's t test.

Figure 6. *Continued*

(D) RT-qPCR analysis of *C21orf2* and *Nek1* mRNA abundance (normalized by that of *Gapdh* mRNA) in parental and VLKI ESCs. Data are means ± SEM for three independent experiments. The p values were determined by Student's t test.

(E) Representative immunofluorescence analysis of parental and VLKI iMNs generated after exposure of the corresponding ESCs to DOX (3 μg/mL) for 2 days. The cells were stained with antibodies to βIII-tubulin (neuronal marker), and the fluorescence of GFP was monitored directly. Scale bar, 50 μm.

(F) Quantification of neurite length for parental and VLKI iMNs in images similar to those in (E). The length of neurites formed by iMNs differentiated from parental and VLKI ESCs was measured in eight wells (n = 8: four wells of a six-well plate in each of two independent experiments). Total neurite length for at least 15 iMNs per well was measured, with the average values being calculated and plotted for each genotype. The internal line and box boundaries indicate the median and quartile values. The p value was determined with Student's t test.

See also Figure S6.

the abundance of the corresponding mRNA (Figure 6D), consistent with our earlier finding that C21ORF2 stabilizes NEK1 (Figure 4). To determine the possible effect of the *C21orf2* mutation on the phenotype of motor neurons, we generated iMNs from VLKI ESCs by exposing the cells to DOX in order to induce expression of NIL factors. Immunoblot analysis of the VLKI cells at 2 days after DOX addition confirmed the accumulation of C21ORF2 and NEK1 compared with the levels of these proteins apparent in parental cells (Figure S6D). We measured the length of neurites formed by the GFP-positive cells and found that the average neurite length for VLKI iMNs was significantly shorter than that for iMNs differentiated from the parental ESCs (Figures 6E and 6F). Although the detailed mechanism underlying this phenotype of VLKI iMNs remains to be determined, the accumulation of C21ORF2 or NEK1 induced by *C21orf2* mutation likely triggers aberrant differentiation or dysfunction of iMNs.

DISCUSSION

Multiple SCF-type ubiquitin ligases play pivotal roles in regulation of the cell cycle and suppression of tumorigenesis, with the functions of these enzymes having been studied mostly in relation to cancer development (Nakayama and Nakayama, 2006; Wang et al., 2014). On the other hand, emerging evidence implicates SCF complexes in the development of several neurodegenerative diseases. Mutations in the F box protein FBXO7 (encoded by *PARK15*), for example, have been shown to give rise to early-onset autosomal recessive Parkinson's disease (Shojaee et al., 2008), and SCF^{FBXL5} has been found to catalyze ubiquitylation of α-synuclein, which contributes to the Lewy body-like pathology of Parkinson's disease (Gerez et al., 2019). In addition, down-regulation of CUL1 and SKP1 has been observed in animal models of Huntington's disease and spinocerebellar ataxia type 3 (SCA3) (Bhutani et al., 2012), and SCF^{FBXO33} modulates the ubiquitylation and solubility of the polyglutamine protein SCA3 (Chen et al., 2019). However, no biological data have been available on the potential role of SCF-type ubiquitin ligases in the pathogenesis of ALS. Although *CCNF*, which encodes cyclin F (also known as FBXO1), is a causative gene of ALS (Williams et al., 2016), we previously found that SCF^{FBXO1} does not mediate the ubiquitylation of other major ALS-related proteins (Yu et al., 2019). We now demonstrate that an SCF-type ubiquitin ligase is associated with ALS pathogenesis by showing that C21ORF2 is a substrate of SCF^{FBXO3} *in vivo*, whereas its ALS-associated mutant V58L is not.

The substrates and biological roles of FBXO3 remain to be fully characterized. FBXO3 regulates gene expression associated with cytokine-driven inflammation as well as bone morphogenetic protein (BMP) signaling by mediating the proteasomal degradation of FBXL2 and SMAD-specific E3 ubiquitin ligase 1 (SMURF1), respectively (Chen et al., 2013; Li et al., 2015; Mallampalli et al., 2013). FBXO3 also increases the transcriptional activity of autoimmune regulator (AIRE) at genes for tissue-specific antigens by mediating its ubiquitylation (Shao et al., 2016). Although the ApaG domain in the COOH terminal region of FBXO3 is indispensable for recognition of FBXL2 (Mallampalli et al., 2013), our results now show that FBXO3 binds to its substrate C21ORF2 not via the ApaG domain but through the region upstream of this domain (Figure 1B). At least 21 conserved homology domains including the ApaG domain have been identified as sites of substrate binding in FBXO-type F box proteins (Jin et al., 2004; Skaar et al., 2013). Our data now indicate that FBXO3 possesses at least one other substrate recognition domain in addition to its ApaG domain. In general, substrate recognition by F box proteins is regulated by posttranslational modification (Skaar et al., 2013). In most cases, phosphorylation of a degron in the substrate facilitates its interaction with the F box protein. Phosphorylation of threonine-404 in FBXL2 and that of threonine-68 and serine-156 in AIRE are thus indispensable for the interaction with FBXO3 (Chen et al., 2013; Shao et al., 2016). However, we have now found that the binding of FBXO3 to C21ORF2 is negatively

regulated by NEK1-catalyzed phosphorylation of C21ORF2, again suggesting that FBXO3 possesses at least two distinct domains for substrate recognition and that these domains differ in their phosphorylation requirement. Binding between an F box protein and its substrate, such as that between FBXO11 and CDT2 or between FBXL2 and p85β (Kuchay et al., 2013; Rossi et al., 2013), has previously been found to be inhibited by substrate phosphorylation.

Functional interaction between C21ORF2 and NEK1 has been previously suggested. The impaired repair of DNA damage apparent in C21ORF2-depleted HeLa cells was thus normalized by overexpression of NEK1 (Fang et al., 2015). In addition, a ciliopathy phenotype of zebrafish induced by injection of a NEK1 antisense morpholino-oligonucleotide was rescued by co-injection of human *C21ORF2* mRNA (Wheway et al., 2015). These studies suggest that C21ORF2 and NEK1 play complementary roles in the same biological pathways. Given that we have now shown that C21ORF2 and NEK1 stabilize each other in a manner dependent on SCF^{FBXO3}, our study may provide a possible explanation for the functional interaction between C21ORF2 and NEK1 observed in HeLa cells and zebrafish. Of note, we found that the V58L mutant of C21ORF2 undergoes excessive phosphorylation by NEK1, which attenuates its interaction with FBXO3 and thereby increases its stability, resulting in turn in the stabilization of NEK1 and in an aberrant motor neuron phenotype. NEK1 is thus a potential target for a kinase inhibitor that might be expected to limit the accumulation of C21ORF2 and thereby rescue neuronal function.

C21ORF2 is widely expressed among tissues, but its function has not been well elucidated (Wang et al., 2016). A reduced level of C21ORF2 expression has been observed in the brain of individuals with Down syndrome (Shim et al., 2003), suggesting that it may play a key role in neurons. *C21ORF2* mutations have been found to cause early-onset retinal dystrophy, Jeune syndrome, and axial spondylometaphyseal dysplasia, the latter of which is also caused by *NEK1* mutations (Khan et al., 2015; Wang et al., 2016, 2017; Wheway et al., 2015). These conditions are all categorized as ciliopathies, given that they result from dysfunction of the primary cilium, a solitary organelle located at the cell surface that regulates various cellular functions (Fliegauf et al., 2007). The proportion of lumbar motor neurons with a primary cilium was found to be reduced in a transgenic mouse model of ALS (Ma et al., 2011). Although the function of the primary cilium of motor neurons remains unknown, the accumulation of C21ORF2 in motor neurons of individuals with ALS-associated *C21ORF2* mutations might induce dysfunction of the primary cilium and thereby contribute to ALS pathogenesis.

We found that stabilization of C21ORF2 protein resulted in an increased abundance of NEK1 and impaired the growth of neurites in iMNs. However, there is no genetic or biological evidence indicating that overexpression of NEK1 leads to dysfunction of motor neurons. Indeed, heterozygous frameshift mutations of *NEK1* have been identified as causal mutations of ALS, suggesting that NEK1 haploinsufficiency gives rise to the development of ALS (Brenner et al., 2016). Consistent with this notion, motor neurons derived from human induced pluripotent stem cells harboring a heterozygous 2434A>T mutation of *NEK1* were found to contain half the normal amount of NEK1 protein and to manifest impairment of DNA damage repair (Higelin et al., 2018). However, the effects of several other ALS-associated missense mutations, such as p.Asn181Ser located in the kinase domain, on NEK1 function remain to be determined. Demonstration that some such missense mutations increase the kinase activity of NEK1 would provide genetic support for our suggestion that overexpression of NEK1 may contribute to the development of ALS.

With regard to potential substrates of NEK1 that might play a role in the pathogenesis of ALS, NEK1 binds ALS2 and vesicle-associated membrane protein B (VAPB), both of which function in the endoplasmic reticulum transport system and are implicated as ALS-related proteins (Cirulli et al., 2015). In addition, kinesin family member 3A (KIF3A) was identified as an interacting protein for NEK1 and harbors putative phosphorylation sites (Surpili et al., 2003). KIF3A is a subunit of the heterotrimeric KIF3 motor complex that is essential for the elongation of neurites and which is down-regulated in the motor cortex of individuals with sporadic ALS (Hirokawa et al., 2009; Pantelidou et al., 2007). It is possible that pathogenic effects of NEK1 haploinsufficiency or hyperactivity are due to altered phosphorylation of these or other proteins.

Together, our data thus show that SCF^{FBXO3} targets C21ORF2 for proteasomal degradation and that the ubiquitylation of C21ORF2 is negatively regulated by NEK1-mediated phosphorylation of C21ORF2. Cross talk between ubiquitylation and phosphorylation thus regulates the abundance of C21ORF2. On the other hand, C21ORF2 suppresses the degradation of NEK1, which means that SCF^{FBXO3} limits the amounts of

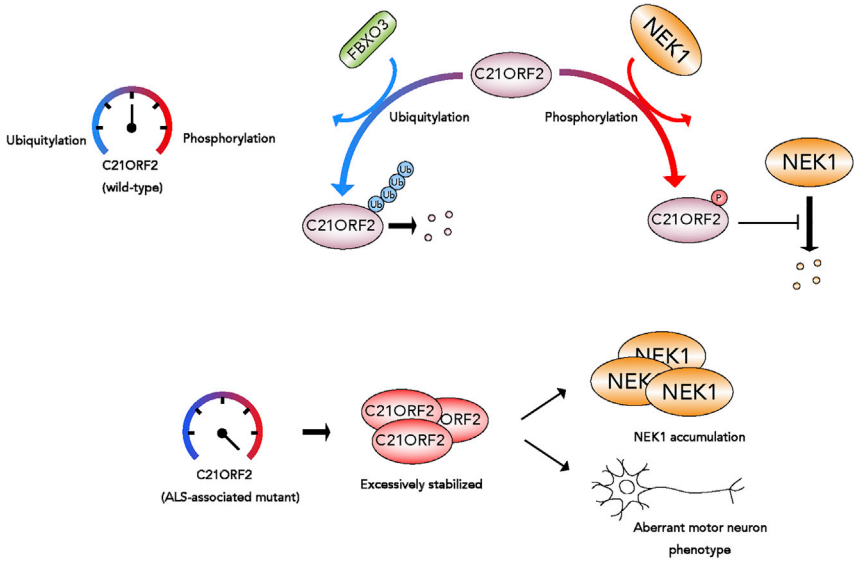

Figure 7. Proposed Model for the Mechanism by Which *C21ORF2* Mutation Might Give Rise to ALS

Cross talk between FBXO3-mediated ubiquitylation and NEK1-catalyzed phosphorylation determines the intracellular abundance of C21ORF2, which in turn stabilizes NEK1. The V58L mutation of *C21ORF2* disrupts the operation of this regulatory system, resulting in the accumulation of both C21ORF2 and NEK1 and giving rise to an aberrant motor neuron phenotype.

both C21ORF2 and NEK1. The ALS-associated V58L mutant of C21ORF2 is more stable than is the WT protein because it is phosphorylated to a greater extent by NEK1 and therefore resistant to ubiquitylation by FBXO3. It therefore mediates more robust inhibition of NEK1 degradation and gives rise to an aberrant phenotype of motor neurons. The accumulation of C21ORF2 and NEK1 thus likely contributes to the pathogenesis of ALS caused by mutation of *C21ORF2* (Figure 7).

Limitations of the Study

The results of this study were obtained with cultured cells. Validation of our findings will thus be required with animal models.

Resource Availability

Lead Contact

Further information and requests for resources and reagents should be directed to and will be fulfilled by the Lead Contact, Keiko Nakayama (nakayak2@med.tohoku.ac.jp).

Materials Availability

All unique and stable reagents generated in this study are available from the Lead Contact with a completed Materials Transfer Agreement.

Data and Code Availability

Original data from replicated experiments have been deposited to Mendeley Data: https://doi.org/10.17632/gg2d67hm43.1.

METHODS

All methods can be found in the accompanying Transparent Methods supplemental file.

SUPPLEMENTAL INFORMATION

Supplemental Information can be found online at https://doi.org/10.1016/j.isci.2020.101491.

ACKNOWLEDGMENTS

This work was supported by KAKENHI grants (15K18365, 17K14955, and 19K07837 to T.N.; 15H05667 and 18K07519 to N.S.; 16H05318 to M.A.; and 18H05215 and 17H04035 to K.N.) from Japan Society for the Promotion of Science (JSPS). We thank Y. Nagasawa and M. Kikuchi for general technical assistance, other laboratory members for discussion, and K. Eggan (Harvard University) for providing mouse ESCs (Hb9::GFP).

AUTHOR CONTRIBUTIONS

Y.W. designed and performed most of the experiments as well as co-wrote the manuscript. T.N. and K.N. directed and coordinated the study, oversaw collection and analysis of the results, and co-wrote the manuscript. M.N. assisted with experiments. T.A., N.S., H.W., and M.A. provided advice. All authors discussed the results and commented on the manuscript.

DECLARATION OF INTERESTS

The authors declare no competing interests.

Received: April 20, 2020
Revised: July 18, 2020
Accepted: August 19, 2020
Published: September 25, 2020

REFERENCES

Ardley, H.C., and Robinson, P.A. (2004). The role of ubiquitin-protein ligases in neurodegenerative disease. Neurodegener. Dis. *1*, 71–87.

Bai, C., Sen, P., Hofmann, K., Ma, L., Goebl, M., Harper, J.W., and Elledge, S.J. (1996). SKP1 connects cell cycle regulators to the ubiquitin proteolysis machinery through a novel motif, F-box. Cell *86*, 263–274.

Bhutani, S., Das, A., Maheshwari, M., Lakhotia, S.C., and Jana, N.R. (2012). Dysregulation of core components of SCF complex in poly-glutamine disorders. Cell Death Dis *3*, e428.

Brenner, D., Muller, K., Wieland, T., Weydt, P., Bohm, S., Lule, D., Hubers, A., Neuwirth, C., Weber, M., Borck, G., et al. (2016). NEK1 mutations in familial amyotrophic lateral sclerosis. Brain. *139*, e28.

Brown, R.H., and Al-Chalabi, A. (2017). Amyotrophic lateral sclerosis. N. Engl. J. Med. *377*, 162–172.

Chen, B.B., Coon, T.A., Glasser, J.R., McVerry, B.J., Zhao, J., Zhao, Y., Zou, C., Ellis, B., Sciurba, F.C., Zhang, Y., et al. (2013). A combinatorial F box protein directed pathway controls TRAF adaptor stability to regulate inflammation. Nat. Immunol. *14*, 470–479.

Chen, Y., Chen, P.L., Chen, C.F., Jiang, X., and Riley, D.J. (2008). Never-in-mitosis related kinase 1 functions in DNA damage response and checkpoint control. Cell Cycle *7*, 3194–3201.

Chen, Z.S., Wong, A.K.Y., Cheng, T.C., Koon, A.C., and Chan, H.Y.E. (2019). FipoQ/FBXO33, a Cullin-1-based ubiquitin ligase complex component modulates ubiquitination and solubility of polyglutamine disease protein. J. Neurochem. *149*, 781–798.

Chia, R., Chio, A., and Traynor, B.J. (2018). Novel genes associated with amyotrophic lateral sclerosis: diagnostic and clinical implications. Lancet Neurol. *17*, 94–102.

Cirulli, E.T., Lasseigne, B.N., Petrovski, S., Sapp, P.C., Dion, P.A., Leblond, C.S., Couthouis, J., Lu, Y.F., Wang, Q., Krueger, B.J., et al. (2015). Exome sequencing in amyotrophic lateral sclerosis identifies risk genes and pathways. Science *347*, 1436–1441.

Fang, X., Lin, H., Wang, X., Zuo, Q., Qin, J., and Zhang, P. (2015). The NEK1 interactor, C21ORF2, is required for efficient DNA damage repair. Acta Biochim. Biophys. Sin. (Shanghai) *47*, 834–841.

Fliegauf, M., Benzing, T., and Omran, H. (2007). When cilia go bad: cilia defects and ciliopathies. Nat. Rev. Mol. Cell Biol. *8*, 880–893.

Fry, A.M., O'Regan, L., Sabir, S.R., and Bayliss, R. (2012). Cell cycle regulation by the NEK family of protein kinases. J. Cell Sci. *125*, 4423–4433.

Gerez, J.A., Prymaczok, N.C., Rockenstein, E., Herrmann, U.S., Schwarz, P., Adame, A., Enchev, R.I., Courtheoux, T., Boersema, P.J., Riek, R., et al. (2019). A cullin-RING ubiquitin ligase targets exogenous alpha-synuclein and inhibits Lewy body-like pathology. Sci. Transl. Med. *11*, eaau6722.

Gratten, J., Zhao, Q., Benyamin, B., Garton, F., He, J., Leo, P.J., Mangelsdorf, M., Anderson, L., Zhang, Z.H., Chen, L., et al. (2017). Whole-exome sequencing in amyotrophic lateral sclerosis suggests NEK1 is a risk gene in Chinese. Genome Med. *9*, 97.

Higelin, J., Catanese, A., Semelink-Sedlacek, L.L., Oeztuerk, S., Lutz, A.K., Bausinger, J., Barbi, G., Speit, G., Andersen, P.M., Ludolph, A.C., et al. (2018). NEK1 loss-of-function mutation induces DNA damage accumulation in ALS patient-derived motoneurons. Stem Cell Res. *30*, 150–162.

Hirokawa, N., Noda, Y., Tanaka, Y., and Niwa, S. (2009). Kinesin superfamily motor proteins and intracellular transport. Nat. Rev. Mol. Cell Biol. *10*, 682–696.

Jin, J., Cardozo, T., Lovering, R.C., Elledge, S.J., Pagano, M., and Harper, J.W. (2004). Systematic analysis and nomenclature of mammalian F-box proteins. Genes Dev. *18*, 2573–2580.

Kenna, K.P., van Doormaal, P.T., Dekker, A.M., Ticozzi, N., Kenna, B.J., Diekstra, F.P., van Rheenen, W., van Eijk, K.R., Jones, A.R., Keagle, P., et al. (2016). NEK1 variants confer susceptibility to amyotrophic lateral sclerosis. Nat. Genet. *48*, 1037–1042.

Khan, A.O., Eisenberger, T., Nagel-Wolfrum, K., Wolfrum, U., and Bolz, H.J. (2015). C21orf2 is mutated in recessive early-onset retinal dystrophy with macular staphyloma and encodes a protein that localises to the photoreceptor primary cilium. Br. J. Ophthalmol. *99*, 1725–1731.

Kinoshita, E., Kinoshita-Kikuta, E., and Koike, T. (2009). Separation and detection of large phosphoproteins using Phos-tag SDS-PAGE. Nat. Protoc. *4*, 1513–1521.

Kuchay, S., Duan, S., Schenkein, E., Peschiaroli, A., Saraf, A., Florens, L., Washburn, M.P., and Pagano, M. (2013). FBXL2- and PTPL1-mediated degradation of p110-free p85beta regulatory subunit controls the PI(3)K signalling cascade. Nat. Cell Biol. *15*, 472–480.

Letwin, K., Mizzen, L., Motro, B., Ben-David, Y., Bernstein, A., and Pawson, T. (1992). A mammalian dual specificity protein kinase, Nek1, is related to the NIMA cell cycle regulator and highly expressed in meiotic germ cells. EMBO J. *11*, 3521–3531.

Li, D., Xie, P., Zhao, F., Shu, J., Li, L., Zhan, Y., and Zhang, L. (2015). F-box protein Fbxo3 targets Smurf1 ubiquitin ligase for ubiquitination and

degradation. Biochem. Biophys. Res. Commun. *458*, 941–945.

Ling, S.C., Polymenidou, M., and Cleveland, D.W. (2013). Converging mechanisms in ALS and FTD: disrupted RNA and protein homeostasis. Neuron *79*, 416–438.

Ma, X., Peterson, R., and Turnbull, J. (2011). Adenylyl cyclase type 3, a marker of primary cilia, is reduced in primary cell culture and in lumbar spinal cord in situ in G93A SOD1 mice. BMC Neurosci. *12*, 71.

Mallampalli, R.K., Coon, T.A., Glasser, J.R., Wang, C., Dunn, S.R., Weathington, N.M., Zhao, J., Zou, C., Zhao, Y., and Chen, B.B. (2013). Targeting F box protein Fbxo3 to control cytokine-driven inflammation. J. Immunol. *191*, 5247–5255.

Mazzoni, E.O., Mahony, S., Closser, M., Morrison, C.A., Nedelec, S., Williams, D.J., An, D., Gifford, D.K., and Wichterle, H. (2013). Synergistic binding of transcription factors to cell-specific enhancers programs motor neuron identity. Nat. Neurosci. *16*, 1219–1227.

McDowell, G.S., and Philpott, A. (2013). Non-canonical ubiquitylation: mechanisms and consequences. Int. J. Biochem. Cell Biol. *45*, 1833–1842.

Melo-Hanchuk, T.D., Slepicka, P.F., Meirelles, G.V., Basei, F.L., Lovato, D.V., Granato, D.C., Pauletti, B.A., Domingues, R.R., Leme, A.F.P., Pelegrini, A.L., et al. (2017). NEK1 kinase domain structure and its dynamic protein interactome after exposure to Cisplatin. Sci. Rep. *7*, 5445.

Nakagawa, T., Nakayama, K., and Nakayama, K.I. (2020). Knockout mouse models provide Insight into the biological functions of CRL1 components. Adv. Exp. Med. Biol. *1217*, 147–171.

Nakayama, K.I., and Nakayama, K. (2006). Ubiquitin ligases: cell-cycle control and cancer. Nat. Rev. Cancer *6*, 369–381.

Neumann, M., Sampathu, D.M., Kwong, L.K., Truax, A.C., Micsenyi, M.C., Chou, T.T., Bruce, J., Schuck, T., Grossman, M., Clark, C.M., et al. (2006). Ubiquitinated TDP-43 in frontotemporal lobar degeneration and amyotrophic lateral sclerosis. Science *314*, 130–133.

Pantelidou, M., Zographos, S.E., Lederer, C.W., Kyriakides, T., Pfaffl, M.W., and Santama, N. (2007). Differential expression of molecular motors in the motor cortex of sporadic ALS. Neurobiol. Dis. *26*, 577–589.

Rossi, M., Duan, S., Jeong, Y.T., Horn, M., Saraf, A., Florens, L., Washburn, M.P., Antebi, A., and Pagano, M. (2013). Regulation of the CRL4(Cdt2) ubiquitin ligase and cell-cycle exit by the SCF(Fbxo11) ubiquitin ligase. Mol. Cell *49*, 1159–1166.

Scott, H.S., Kyriakou, D.S., Peterson, P., Heino, M., Tahtinen, M., Krohn, K., Chen, H., Rossier, C., Lalioti, M.D., and Antonarakis, S.E. (1998). Characterization of a novel gene, C21orf2, on human chromosome 21q22.3 and its exclusion as the APECED gene by mutation analysis. Genomics *47*, 64–70.

Shahheydari, H., Ragagnin, A., Walker, A.K., Toth, R.P., Vidal, M., Jagaraj, C.J., Perri, E.R., Konopka, A., Sultana, J.M., and Atkin, J.D. (2017). Protein quality control and the amyotrophic lateral sclerosis/frontotemporal dementia continuum. Front. Mol. Neurosci. *10*, 119.

Shao, W., Zumer, K., Fujinaga, K., and Peterlin, B.M. (2016). FBXO3 protein promotes ubiquitylation and transcriptional activity of AIRE (autoimmune regulator). J. Biol. Chem. *291*, 17953–17963.

Shim, K.S., Bergelson, J.M., Furuse, M., Ovod, V., Krude, T., and Lubec, G. (2003). Reduction of chromatin assembly factor 1 p60 and C21orf2 protein, encoded on chromosome 21, in Down syndrome brain. J. Neural Transm. (*Suppl*), 117–128.

Shojaee, S., Sina, F., Banihosseini, S.S., Kazemi, M.H., Kalhor, R., Shahidi, G.A., Fakhrai-Rad, H., Ronaghi, M., and Elahi, E. (2008). Genome-wide linkage analysis of a Parkinsonian-pyramidal syndrome pedigree by 500 K SNP arrays. Am. J. Hum. Genet. *82*, 1375–1384.

Skaar, J.R., Pagan, J.K., and Pagano, M. (2013). Mechanisms and function of substrate recruitment by F-box proteins. Nat. Rev. Mol. Cell Biol. *14*, 369–381.

Surpili, M.J., Delben, T.M., and Kobarg, J. (2003). Identification of proteins that interact with the central coiled-coil region of the human protein kinase NEK1. Biochemistry *42*, 15369–15376.

Thiel, C., Kessler, K., Giessl, A., Dimmler, A., Shalev, S.A., von der Haar, S., Zenker, M., Zahnleiter, D., Stoss, H., Beinder, E., et al. (2011). NEK1 mutations cause short-rib polydactyly syndrome type majewski. Am. J. Hum. Genet. *88*, 106–114.

van Rheenen, W., Shatunov, A., Dekker, A.M., McLaughlin, R.L., Diekstra, F.P., Pulit, S.L., van der Spek, R.A., Vosa, U., de Jong, S., Robinson, M.R., et al. (2016). Genome-wide association analyses identify new risk variants and the genetic architecture of amyotrophic lateral sclerosis. Nat. Genet. *48*, 1043–1048.

Velasco, S., Ibrahim, M.M., Kakumanu, A., Garipler, G., Aydin, B., Al-Sayegh, M.A., Hirsekorn, A., Abdul-Rahman, F., Satija, R., Ohler, U., et al. (2017). A multi-step transcriptional and chromatin state cascade underlies motor neuron programming from embryonic stem cells. Cell Stem Cell *20*, 205–217.e8.

Wang, Z., Horemuzova, E., Iida, A., Guo, L., Liu, Y., Matsumoto, N., Nishimura, G., Nordgren, A., Miyake, N., Tham, E., et al. (2017). Axial spondylometaphyseal dysplasia is also caused by NEK1 mutations. J. Hum. Genet. *62*, 503–506.

Wang, Z., Iida, A., Miyake, N., Nishiguchi, K.M., Fujita, K., Nakazawa, T., Alswaid, A., Albalwi, M.A., Kim, O.H., Cho, T.J., et al. (2016). Axial spondylometaphyseal dysplasia is caused by C21orf2 mutations. PLoS One *11*, e0150555.

Wang, Z., Liu, P., Inuzuka, H., and Wei, W. (2014). Roles of F-box proteins in cancer. Nat. Rev. Cancer *14*, 233–247.

Weishaupt, J.H., Hyman, T., and Dikic, I. (2016). Common molecular pathways in amyotrophic lateral sclerosis and frontotemporal dementia. Trends Mol. Med. *22*, 769–783.

Wheway, G., Schmidts, M., Mans, D.A., Szymanska, K., Nguyen, T.T., Racher, H., Phelps, I.G., Toedt, G., Kennedy, J., Wunderlich, K.A., et al. (2015). An siRNA-based functional genomics screen for the identification of regulators of ciliogenesis and ciliopathy genes. Nat. Cell Biol. *17*, 1074–1087.

Wichterle, H., Lieberam, I., Porter, J.A., and Jessell, T.M. (2002). Directed differentiation of embryonic stem cells into motor neurons. Cell *110*, 385–397.

Williams, K.L., Topp, S., Yang, S., Smith, B., Fifita, J.A., Warraich, S.T., Zhang, K.Y., Farrawell, N., Vance, C., Hu, X., et al. (2016). CCNF mutations in amyotrophic lateral sclerosis and frontotemporal dementia. Nat. Commun. *7*, 11253.

Yu, Y., Nakagawa, T., Morohoshi, A., Nakagawa, M., Ishida, N., Suzuki, N., Aoki, M., and Nakayama, K. (2019). Pathogenic mutations in the ALS gene CCNF cause cytoplasmic mislocalization of Cyclin F and elevated VCP ATPase activity. Hum. Mol. Genet. *28*, 3486–3497.

iScience, Volume *23*

Supplemental Information

An Amyotrophic Lateral Sclerosis-Associated Mutant of C21ORF2 Is Stabilized by NEK1-Mediated Hyperphosphorylation and the Inability to Bind FBXO3

Yasuaki Watanabe, Tadashi Nakagawa, Tetsuya Akiyama, Makiko Nakagawa, Naoki Suzuki, Hitoshi Warita, Masashi Aoki, and Keiko Nakayama

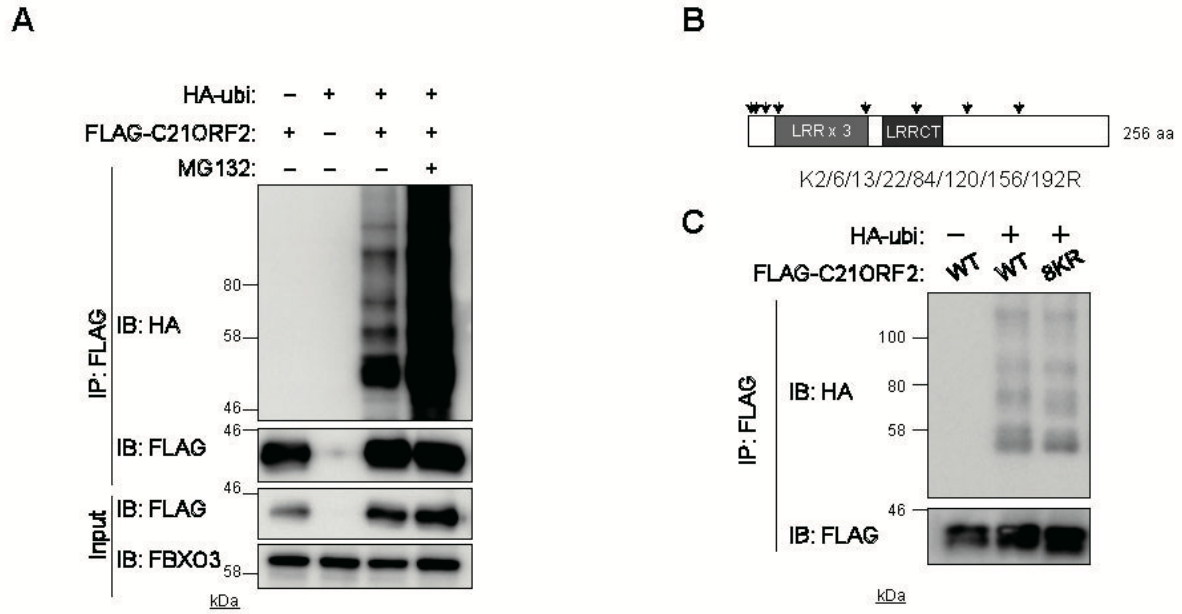

Figure S1. C21ORF2 Is Ubiquitylated for Proteasomal Degradation in a Lysine-Independent Manner, Related to Figure 1

(A**)** HEK293T cells expressing HA-ubiquitin and FLAG-C21ORF2, as indicated, were incubated with 10 μM MG132 or DMSO vehicle for 4 h and were then assayed for in vivo ubiquitylation of FLAG-C21ORF2 as in Figure 1E.

(B) Schematic representation of the 8KR mutant of human C21ORF2, in which all eight lysine residues are replaced with arginine. The three LRR domains and the LRR COOH-terminal (LRRCT) domain are shown.

(C) Lysates of HEK293T cells expressing HA-ubiquitin and FLAG-C21ORF2 (WT or 8KR), as indicated, were subjected to immunoprecipitation with antibodies to FLAG, and the resulting precipitates were subjected to immunoblot analysis with antibodies to HA and to FLAG.

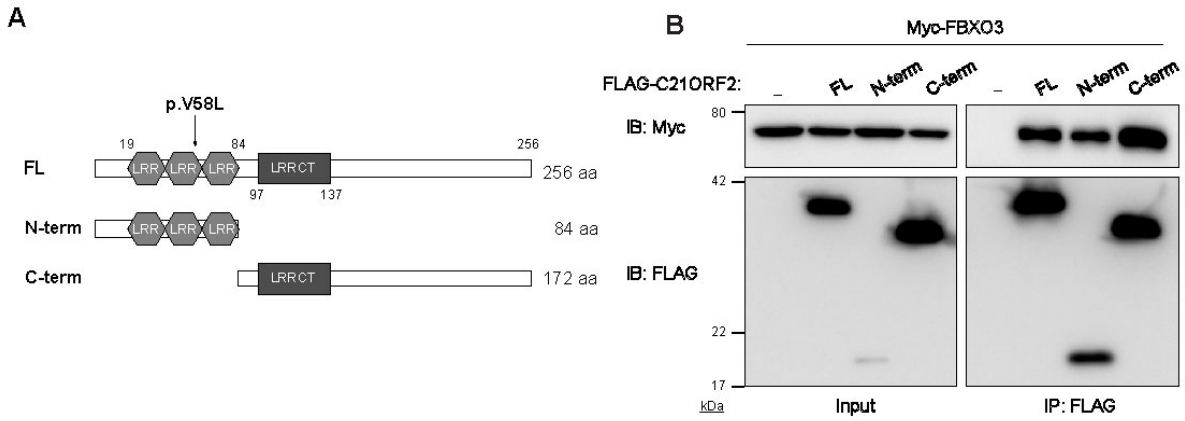

Figure S2. FBXO3 Binds to a Broad Region of C21ORF2, Related to Figure 2

(A) Schematic representation of truncated variants of human C21ORF2.

(B) Immunoprecipitation and immunoblot analysis of the interaction of FLAG-tagged C21ORF2 variants (FL, N-term, or C-term) with Myc-tagged FBXO3 in HEK293T cells.

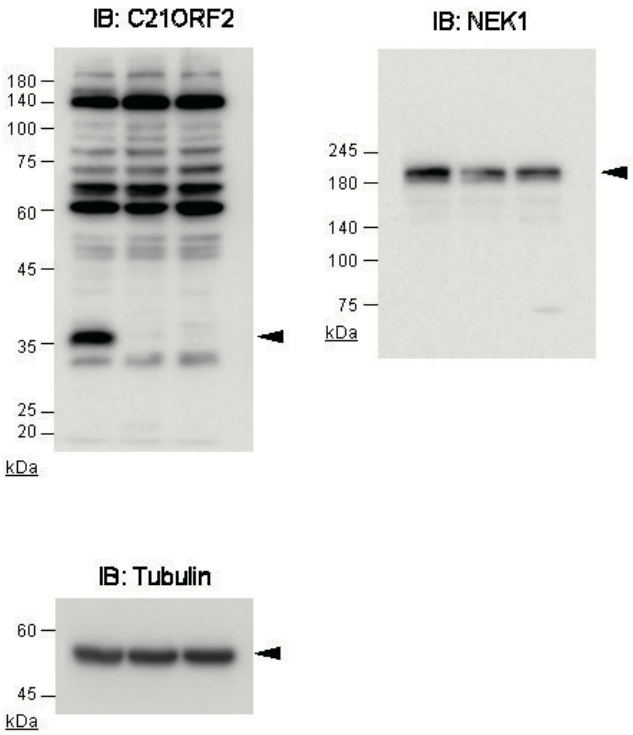

Figure S3. Original Uncropped Immunoblots of Figure 4A, Related to Figure 4

Arrowheads indicate specific immunoreactive proteins.

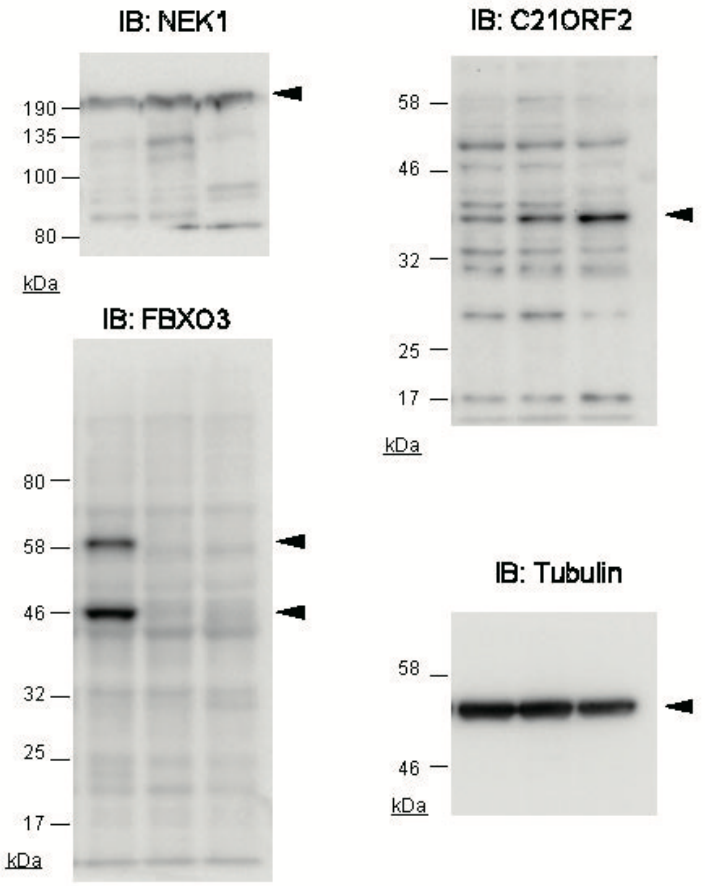

Figure S4. Original Uncropped Immunoblots of Figure 5A, Related to Figure 5

Arrowheads indicate specific immunoreactive proteins.

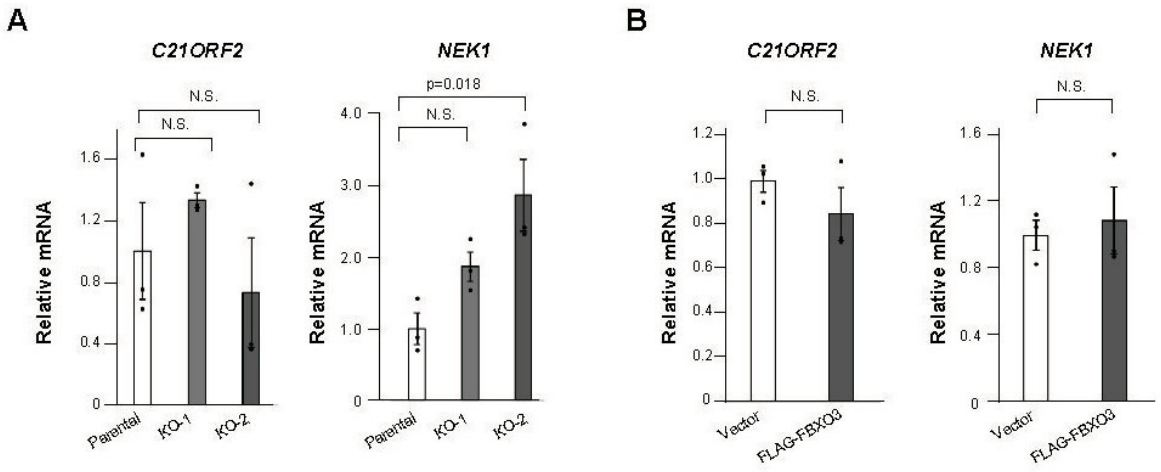

Figure S5. Expression of *C21ORF2* and *NEK1* in *FBXO3* KO Cells, Related to Figure 5

(A) RT-qPCR analysis of *C21ORF2* and *NEK1* mRNA abundance (normalized by that of *GAPDH* mRNA) in parental cells and in two *FBXO3* KO clones of SH-SY5Y cells. Data are means ± SEM for three independent experiments. The p values were determined by one-way ANOVA followed by Tukey's post hoc test.

(B) RT-qPCR analysis of *C21ORF2* and *NEK1* mRNA abundance (normalized by that of *GAPDH* mRNA) in *FBXO3* KO cells infected with a lentivirus encoding FLAG-FBXO3 or with the corresponding empty virus (Vector). Data are means ± SEM for three independent experiments. N.S., Student's t test.

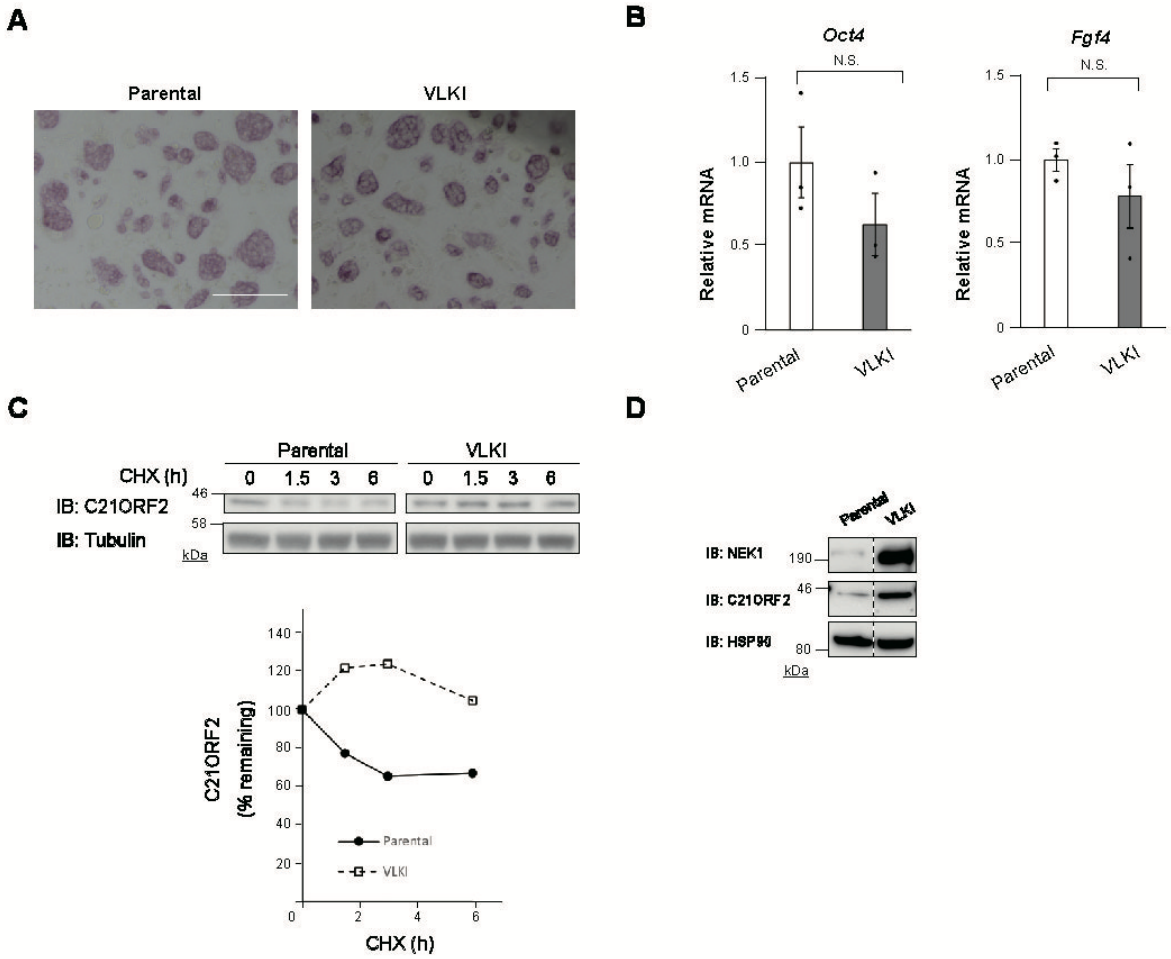

Figure S6. Characterization of VLKI ESCs, Related to Figure 6

(A) Alkaline phosphatase staining of parental (DOX-NIL) and VLKI ESCs cultured on feeder cells. Scale bar, 500 μm.

(B) RT-qPCR analysis of *Oct4* and *Fgf4* mRNA abundance (normalized by that of *Gapdh* mRNA) in parental and VLKI ESCs. Data are means ± SEM for three independent experiments. N.S., Student's t test.

(C) Parental and VLKI ESCs were treated with cycloheximide (25 μg/ml) for the indicated times, lysed, and subjected to immunoblot analysis with antibodies to C21ORF2 (top). The remaining percentage of C21ORF2 (normalized by the amount of α-tubulin) was determined by densitometry (bottom).

(D) Immunoblot analysis of C21ORF2 and NEK1 in parental and VLKI iMNs formed after exposure of the corresponding ESCs to DOX (3 μg/ml) for 2 days.

Table S1. Primers for RT-qPCR Analysis, Related to Figure 4 and Figure S6

Gene	Primer sequence (5'→3')	Direction
C21orf2 (mouse)	CAGCTCTGCAACTGAGACCA	Forward
	GGCAGTCAGGATGTTCCTATTCT	Reverse
Nek1 (mouse)	CCTGGCCAAGCCACCTC	Forward
	ACAAACACAGCGGTTCTGA	Reverse
C21ORF2 (human)	CCCAGGGTGAAGACAGTCAC	Forward
	TCCACCCTCTATGTCCCGAG	Reverse
NEK1 (human)	ACGTCCTGTGTCACTGAGTTTT	Forward
	ACATACTGTCTGCCATCTTCTGT	Reverse
Oct4 (mouse)	GATGCTGTGAGCCCAAGGCAAG	Forward
	GGCTCCTGATCAACAGCATCAC	Reverse
Fgf4 (mouse)	GAGGCGTGGTGAGCATCTT	Forward
	ACACTCGGTTCCCCTTCTTG	Reverse
GAPDH (human)	AGGTGAAGGTCGGAGTCAAC	Forward
	GACAAGCTTCCCGTTCTCAG	Reverse
Gapdh (mouse)	CCAATGTGTCCGTCGTGGATCT	Forward
	GTTGAAGTCGCAGGAGACAACC	Reverse

TRANSPARENT METHODS

Cell culture

HEK293T (ATCC, CRL-3216) and SH-SY5Y (ATCC, CRL-2266) cells were maintained in Dulbecco's modified Eagle's medium (DMEM) supplemented with 10% fetal bovine serum (FBS), penicillin (50 U/ml), streptomycin (50 μg/ml), 2 mM L-glutamine, 1% MEM–nonessential amino acids, and 1% sodium pyruvate (Thermo Fisher Scientific). Mouse ESCs (kindly provided by K. Eggan, University of Harvard) were maintained with mitomycin C–treated MEF (DR4) feeder cells (ATCC, CRL-1045) in ES culture medium consisting of DMEM supplemented with 15% Hyclone FBS (Thermo Fisher Scientific), penicillin (50 U/ml), streptomycin (50 μg/ml), 2 mM L-glutamine, 1% MEM–nonessential amino acids, 1% sodium pyruvate, 0.1 mM β-mercaptoethanol, recombinant leukemia inhibitory factor (LIF, 1000 U/ml) (EMD Millipore), 3 μM CHIR99021 (Stemgent), and 1 μM PD0325901 (Stemgent). The medium was changed every day.

Construction of plasmids

For generation of transient expression vectors, cDNAs encoding human C21ORF2, FBXO3, and NEK1 were amplified from HEK293T or HeLa cells, cloned into pENTR (Thermo Fisher Scientific), and verified by sequencing. The resulting vectors were subjected to recombination with various destination plasmids with the use of LR clonase II (Thermo Fisher Scientific) in order to obtain expression plasmids for the corresponding FLAG-, HA-, or Myc epitope–tagged proteins. Point and deletion mutants were generated by PCR-based mutagenesis. For generation of a lentivirus encoding FLAG-FBXO3, the corresponding cDNA was inserted into CSII-EF-MCS (Riken BRC #RDB04378) together with a puromycin resistance gene. For generation of lentiviruses for DOX-inducible C21ORF2 constructs, cDNA encoding HA-C21ORF2 (WT or V58L) was cloned into pEN_TTGmiRc2 (Addgene #25753) after removal of the coding regions for EGFP and miR-30a with the use of restriction enzymes. The resulting vectors were subjected to recombination with the pSLIK-neo destination plasmid (Addgene #25735). For generation of a lentivirus for DOX-inducible NIL factors

(NGN2, ISL1, LHX3), human cDNAs encoding the NIL factors were amplified with or without overhangs containing the sequence encoding the 2A self-cleaving peptide and were then cloned into the same modified pEN_TTGmiRc2 vector. The resulting vector was subjected to recombination with pSLIK-neo. Bacterial expression vectors were constructed by insertion of FBXO3 cDNA into pGEX-6P-3 (Addgene #27-4599-01) and of cDNA encoding C21ORF2 (WT or V58L) into pET30a (Novagen #69909-3). For construction of Cas9-sgRNA plasmids, the single guide RNAs (sgRNAs) were designed with the use of the CRISPR Design Tool (http://crispr.mit. edu) or CRISPRdirect (https://crispr.dbcls.jp), and the corresponding DNA sequences were subcloned into pSpCas9(BB)-2A-Puro(PX459) V2.0 (Addgene #62988) (Ran et al., 2013).

Cell transfection

HEK293T and SH-SY5Y cells were transiently transfected with plasmid DNA with the use of the PEI MAX (Polysciences) and FuGENE HD (Promega) reagents, respectively. HEK293T cells were transfected with human NEK1 (Ambicon silencer select s9442 and s9443) or negative control (medium GC,Thermo Fisher Scientific) siRNAs with the use of the RNAiMax reagent (Thermo Fisher Scientific).

Immunoprecipitation and immunoblot analysis

Cells were washed with phosphate-buffered saline (PBS) and lysed for 10 min at 4°C in NP-40 lysis buffer [0.5% Nonidet P-40, 50 mM Tris-HCl (pH 7.5), 150 mM NaCl, 10% glycerol] supplemented with a protease inhibitor cocktail [aprotinin (10 μg/ml) (Sigma), leupeptin (10 μg/ml) (Peptide institute), 1 mM phenylmethylsulfonyl fluoride (Wako)]. The lysates were centrifuged at 20,000 × *g* for 15 min at 4°C to remove debris, and the resulting supernatants were subjected to immunoprecipitation or direct immunoblot analysis. For immunoblot analysis, lysate supernatants were mixed with Laemmli buffer and fractionated by SDS-PAGE, the separated proteins were transferred to a polyvinylidene difluoride membrane, and the membrane was incubated first with primary antibodies and then with horseradish

peroxidase (HRP)–conjugated secondary antibodies to mouse or rabbit immunoglobulin G (IgG). Immune complexes were detected with the ChemiDoc Touch System (Bio-Rad). For immunoprecipitation, the lysate supernatants were incubated with Dynabeads Protein G (Life Technologies) conjugated with antibodies to FLAG or to Myc. The resulting immunoprecipitates were washed three times with PBS containing 0.1% Triton X-100 and 10% glycerol and were then subjected to immunoblot analysis. Relative band intensities were quantified by densitometry with the use of ImageJ (Schneider et al., 2012).

Cycloheximide chase analysis

Cells were incubated with cycloheximide (25 μg/ml) (Sigma) for the indicated times and then subjected to immunoblot analysis.

In vivo ubiquitylation assay

HEK293T cells transfected with expression vectors for HA-ubiquitin (in house), Myc epitope–tagged FBXO3 (WT or mutant), and FLAG-tagged C21ORF2 (WT or mutant) were lysed with NP-40 lysis buffer under denaturing conditions (0.1% SDS) for disruption of noncovalent protein-protein interactions, and the lysates were subjected to immunoprecipitation with antibodies to FLAG followed by immunoblot analysis with the indicated antibodies (Nakagawa et al., 2015).

In vitro binding assay

Recombinant GST-tagged FBXO3 (2 μg/ml) and recombinant His_6-tagged C21ORF2 (WT or V58L, 20 ng/ml) that had been expressed in and purified from *E. coli* BL21 (DE3) (Agilent Technologies) were incubated overnight at 4°C with rotation, after which GST-FBXO3 was precipitated with glutathione-agarose beads. The resulting precipitates were subjected to immunoblot analysis with antibodies to His_6 and to GST.

RNA isolation and RT-qPCR analysis

RNA was isolated from cells with the use of an SV Total RNA isolation system (Promega) and was subjected to RT with a PrimeScript RT reagent kit (Takara Bio). The resulting cDNA was subjected to real-time PCR analysis with a StepOnePlus real-time PCR system (Life Technologies) and Fast SYBR Green Master Mix (Thermo Fisher Scientific). The sequences of PCR primers are listed in Table S1. Data were analyzed according to the $2^{-\Delta\Delta CT}$ method and were normalized by the amount of mouse or human GAPDH mRNA.

In vitro assay of phosphorylation

HEK293T cells were transiently transfected with an expression vector for Myc epitope–tagged NEK1-N811 (WT or K33R), and the Myc-tagged proteins were immunoprecipitated and purified with the use of a c-Myc Tagged Protein Mild Purification Kit ver. 2 (MBL). His_6-C21ORF2 (WT or V58L, 100 ng) that had been expressed in and purified from bacteria was incubated for 15 min at 30°C with the purified Myc–NEK1-N811 (100 ng) in 30 μl of kinase assay buffer [1 mM EGTA, 25 mM Tris-HCl (pH 7.6), 10 mM $MgCl_2$, 5 mM β-glycerophosphate, 0.5 mM Na_3VO_4, 2.5 mM dithiothreitol, 0.01% Triton-X100, 0.1 mM ATP]. For detection of the mobility shift of phosphorylated proteins, the reaction mixtures were subjected to SDS-PAGE on 8% acrylamide gels containing 65 μM Phos-tag (Wako). The effects of λ phosphatase (New England Biolabs) were examined as described by the manufacturer. Molecular mass markers for Phos-tag gels were not available, but data were interpreted by comparison of immunoblots with or without Phos-tag.

Generation of cell lines by lentivirus transduction

For persistent expression of FLAG-FBXO3 in *FBXO3* KO SH-SY5Y cells, lentiviruses were produced in HEK293T cells cotransfected with the packaging plasmids pCAG-HIVgp (Riken BRC #RDB04394) and pCMV-VSV-G-RSV-Rev (Riken BRC #RDB04393) as well as with CSII-EF-MCS harboring FLAG-FBXO3 cDNA and a puromycin resistance gene (Miyoshi et al., 1998). Culture supernatant

containing the released lentiviruses was added to the medium of *FBXO3* KO SH-SY5Y cells together with polybrene (8 μg/ml) (Sigma). The infected cells were selected by treatment with puromycin (2 μg/ml) for 2 days. DOX-C21ORF2 SH-SY5Y cells and DOX-NIL ESCs were generated by infection with corresponding lentiviruses in the presence of polybrene (8 μg/ml) followed by G418 selection (500 μg/ml) for at least 7 days. The lentiviruses were produced by transfection of HEK293T cells with pSLIK-neo encoding rtTA-TRE–regulated HA-C21ORF2 or NIL factors together with the packaging and pseudotyping plasmids psPAX2 (Addgene #12260) and pMD2.G (Addgene #12259) (Shin et al., 2006).

DOX-inducible generation of iMNs and immunofluorescence analysis

The generation of iMNs from DOX-NIL ESCs was performed as described previously (Velasco et al., 2017), with some modifications. To obtain embryoid bodies, we collected ESCs by treatment with trypsin and seeded them in AK medium consisting of Advanced DMEM-F12:Neurobasal (1:1) medium, 10% KnockOut SR (Thermo Fisher Scientific), penicillin (50 U/ml), streptomycin (50 μg/ml), 2 mM L-glutamine, and 0.1 mM 2-mercaptoethanol. The embryoid bodies were subsequently dissociated by incubation for 20 min at 37°C with TrypLE Express (Thermo Fisher Scientific), and the dissociated cells were passed through a 70-μm cell strainer (BD Falcon). The cells (5×10^4 per well) were transferred to six-well plates containing iMatrix-511(Wako)–coated cover glasses. Expression of NIL factors was induced by the addition of DOX (3 μg/ml) to culture medium supplemented with brain-derived neurotrophic factor (50 ng/ml) (Peprotech). After 2 days, the cells were fixed with 4% paraformaldehyde in PBS, permeabilized with 1% Triton X-100, and exposed for 60 min to 2% bovine serum albumin in PBS. The cells were then incubated for 16 h at 4°C with antibodies to βIII-tubulin, washed twice with PBS containing 0.1% Tween-20, and incubated for 45 min at room temperature with AlexaFluor 546–conjugated secondary antibodies to mouse IgG. Fluorescence images were acquired with a Nikon C2si microscope. Neurite length of the iMNs was measured semiautomatically with the use of NeuronJ software, an ImageJ plugin (Meijering et al., 2004). Staining of ESCs for

alkaline phosphatase was carried out with the use of an Alkaline Phosphatase Staining Kit II (ReprocelI).

Gene knockout by CRISPR/nonhomologous end joining (NHEJ)

The target sequences of sgRNAs were 5'-GCCTGGAGGTGATCACGCTC -3' within exon 3 of *C21ORF2* and 5'-TAGGGTCAGCGGCGCCGTCT-3' within exon 1 of *FBXO3*. HEK293T and SH-SY5Y cells were transiently transfected with the corresponding Cas9-sgRNA plasmid and were treated with puromycin (10 and 5 μg/ml, respectively) for 2 days. The surviving cells were then cloned by the limiting dilution method. The resulting single cell–derived clones were expanded, and their DNA was extracted for genomic PCR analysis and sequencing.

Genome engineering by CRISPR/homology-directed repair (HDR)

A sgRNA was designed to target the sequence 5'-CTGTTGAGGCACGTAAGCCC-3' within intron 4 of *C21orf2*. To induce homologous recombination, we introduced the Cas9-sgRNA plasmid together with a linearized template vector containing *C21orf2* mutant homology arms and a hygromycin resistance gene flanked by LoxP sites into DOX-NIL ESCs by electroporation with a 4D-Nucleofector (Lonza). After 24 h, the cells were selected by treatment with hygromycin (100 μg/ml) for 7 days. An expression vector containing Cre recombinase cDNA and a puromycin resistance gene (in house) was introduced into the surviving cells by electroporation in order to remove the hygromycin resistance gene. After 24 h, the cells were treated with puromycin (3 μg/ml) for 1 day, and the surviving colonies were cloned by the colony pick-up method. Individual clones were expanded, and their DNA was extracted for genomic PCR analysis and sequencing.

Antibodies

Antibodies to βIII-tubulin (ab7751) were obtained from Abcam; those to SKP1 (12248), to RBX1 (11922), and to β-actin (3700) were from Cell Signaling Technology; and those to Myc (sc-40), to

NEK1 (SC-398813), and to FBXO3 (SC-514625) were from Santa Cruz Biotechnology. HRP-conjugated antibodies to HA (11667475001) were from Roche. Antibodies to FLAG (F4042), HRP-conjugated antibodies to FLAG (A8592), and antibodies to α-tubulin (T6074) were obtained from Sigma-Aldrich. Antibodies to Myc (562-5) were from MBL; those to CUL1 (32-2400) were from Life Technologies; those to HSP90 (610418) were from BD Biosciences; and those to GST (R4TM1222100) and to His_6 (R4-TP1111100) were from Recenttec. HRP-conjugated antibodies to mouse IgG (W4021) and to rabbit IgG (W4011) were from Promega. AlexaFluor 546–conjugated antibodies to mouse IgG were obtained from Molecular Probes. HRP-conjugated Mouse TrueBlot ULTRA (18-8817-33) was from Rockland. For detection of human C21ORF2, antibodies were obtained from Proteintech (27609-1-AP) and Genetex (GTX119046). For detection of mouse C21ORF2, antibodies were produced in house.

Statistical analysis

All experiments for statistical analysis were performed at least three times. Data were analyzed with the unpaired two-tailed Student's t test for comparisons between two groups, or by one-way analysis of variance (ANOVA) followed by Tukey's post hoc test for comparisons among three groups. Time courses were compared by two-way ANOVA. Data are presented as means ± SEM, and a p value of <0.05 was considered statistically significant.

SUPPLEMENTAL REFERENCES

Meijering, E., Jacob, M., Sarria, J.C., Steiner, P., Hirling, H., and Unser, M. (2004). Design and validation of a tool for neurite tracing and analysis in fluorescence microscopy images. Cytometry A *58*, 167-176.

Miyoshi, H., Blomer, U., Takahashi, M., Gage, F.H., and Verma, I.M. (1998). Development of a self-inactivating lentivirus vector. J Virol *72*, 8150-8157.

Nakagawa, T., Lv, L., Nakagawa, M., Yu, Y., Yu, C., D'Alessio, A.C., Nakayama, K., Fan, H.Y., Chen, X., and Xiong, Y. (2015). CRL4(VprBP) E3 ligase promotes monoubiquitylation and chromatin binding of TET dioxygenases. Mol Cell *57*, 247-260.

Ran, F.A., Hsu, P.D., Wright, J., Agarwala, V., Scott, D.A., and Zhang, F. (2013). Genome engineering using the CRISPR-Cas9 system. Nat Protoc *8*, 2281-2308.

Schneider, C.A., Rasband, W.S., and Eliceiri, K.W. (2012). NIH Image to ImageJ: 25 years of image analysis. Nat Methods *9*, 671-675.

Shin, K.J., Wall, E.A., Zavzavadjian, J.R., Santat, L.A., Liu, J., Hwang, J.I., Rebres, R., Roach, T., Seaman, W., Simon, M.I.*, et al.* (2006). A single lentiviral vector platform for microRNA-based conditional RNA interference and coordinated transgene expression. Proc Natl Acad Sci U S A *103*, 13759-13764.